Process Safety and Environmental Protection 179 (2023) 10–26

Contents lists available at ScienceDirect

Process Safety and Environmental Protection

journal homepage: www.journals.elsevier.com/process-safety-and-environmental-protection

Gas turbine-based system taking advantage of LNG regasification process for multigeneration purposes; Techno-economic-environmental analysis and machine learning optimization

Yinquan Hu [a], Samir I. Badrawi [b], Jitendra Kumar [c,*], Hala Najwan Sabeh [d], Theyab R. Alsenani [e,*], Fahid Riaz [f], Tamim Alkhalifah [g], Salem Alkhalaf [g], Fahad Alturise [g]

[a] School of Intelligent Manufacturing and Traffic, Chongqing Vocational Institute of Engineering, Chongqing 402260, China
[b] Department of Intelligent Medical Systems, Al Mustaqbal University, 51001 Hilla, Babylon, Iraq
[c] Department of Electronics and Communication Engineering, GLA University, Mathura 281406, Utter Pradesh, India
[d] Information Technology Department, Faculty of Applied Science, Tishk International University, Erbil, Iraq
[e] Department of Electrical Engineering, College of Engineering in Al-Kharj, Prince Sattam Bin Abdulaziz University, Al-Kharj 11942, Saudi Arabia
[f] College of Engineering, Abu Dhabi University, Abu Dhabi, United Arab Emirates
[g] Department of Computer, College of Science and Arts in Ar Rass, Qassim University, Ar Rass, Qassim, Saudi Arabia

ARTICLE INFO

Keywords:
Machine learning
Hydrogen production
Heat recovery
LNG usage
Absorption chiller

ABSTRACT

It is viable for engineers to determine how thermodynamic systems can benefit from heat recovery in order to improve efficiency, reduce costs, and lower carbon dioxide emissions. The authors of the study propose a new energy system that incorporates various cycles and units, including gas turbines, Rankine and two organic Rankine cycles, an absorption refrigeration unit, a proton exchange membrane (PEM) electrolyzer, and a liquefied natural gas (LNG) unit. The hydrogen produced is stored and transferred for use as fuel. The system was modeled and optimized using MATLAB programming software, with a parametric study and sensitivity analysis conducted before employing a genetic algorithm optimization to find the most suitable performance conditions. Modifying the compressor's pressure ratio within the range of 6–18 caused a shift in the cooling load, ranging from 45 to 36 MW. Nonetheless, these adjustments in pressure ratio yielded a reduction of 0.4 Cent/kWh in levelized cost of electricity (LCOE) and 0.15 \$/kg in levelized cost of hydrogen (LCOH). In the base design mode, the total cost rate is 5715.3 \$/h, the exergy efficiency is 39.03%, and the normalized CO_2 emissions are 335.89 kg/GJ. However, the optimization results showed a reduced total cost rate of 1884.50 \$/h, along with an improved exergy efficiency from 39.03% to 40.32% and a decrease in annual CO_2 emissions from 211,000 metric tons to 175,000 metric tons. The implementation of artificial neural networks (ANN) has significantly decreased the time required for optimization from 47 h to just 16 min.

1. Introduction

The combination of a gas turbine cycle and liquefied natural gas (LNG) regasification process, along with Combined Coolant, Heat, and Power (CCHP), can provide numerous benefits for energy production. Firstly, the gas turbine power plant provides reliable and efficient electricity generation, while the LNG regasification process unlocks a clean and versatile fuel source for the plant. Secondly, this combination allows for cost-effective operation by leveraging the high efficiency of gas turbines and the flexibility of LNG. Thirdly, CCHP systems can further optimize efficiency by utilizing waste heat from the gas turbines to provide heating and cooling to nearby buildings or industrial processes. Fourthly, by using LNG as a fuel source, this system replaces traditional fossil fuels, such as oil and coal, with cleaner-burning natural gas, reducing emissions and enhancing environmental stewardship. Fifthly, this integrated approach also enhances energy security by providing access to remote locations without extensive infrastructure. Finally, the combination of gas turbine power plants, LNG regasification, and CCHP offers a robust and sustainable energy solution that can support economic growth while minimizing environmental impact.

* Corresponding authors.
E-mail addresses: jitendra.kumar@gla.ac.in (J. Kumar), t.alsenani@psau.edu.sa (T.R. Alsenani).

https://doi.org/10.1016/j.psep.2023.08.068
Received 16 May 2023; Received in revised form 3 August 2023; Accepted 23 August 2023
Available online 26 August 2023
0957-5820/© 2023 Institution of Chemical Engineers. Published by Elsevier Ltd. All rights reserved.

1.1. Literature review

Gas turbines are tremendously employed in industry for electric power production. In most cases, they are integrated with Steam Rankine Cycles (SRCs) to improve their efficiencies and use the maximum value of input exergy (Maheshwari and Singh, 2019). Gas turbines can also be combined with other components as have been analyzed and their performance have been evaluated in the case of being integrated to vapor injection and Organic Rankine Cycle (ORC) bottoming (Xiao et al., 2021) or biomass gasifier (Khanmohammadi et al., 2015). Additionally, O. Olumayegun et. al (Olumayegun et al., 2016). have generally investigated closed-loop gas turbine cycles in a review paper, in which developments, challenges, and future of these kind of gas turbines are addressed. Zhao et al. (2019) also reviewed the expansion devices in low temperature ORCs. R. Zahedi et. al (Zahedi et al., 2021). performed a comprehensive examination of a system including solar-based unit, biogas, steam, and organic Rankine cycles.

Heat recovery in gas turbine power plants involves capturing waste heat generated during electricity generation and using it for various purposes. This includes combined heat and power (CHP) systems, where the waste heat is used to generate additional energy in the form of steam or hot water for heating buildings or industrial processes. Heat exchangers transfer waste heat to a working fluid, which can be used for heating or other processes. Supplementary firing and bottoming cycles are also employed to increase temperature and generate more electricity. These heat recovery technologies improve overall efficiency, enhance sustainability, and reduce fuel consumption and emissions. This method also is considered for operating several ORC units to generate power, as well as an absorption chiller cycle to produce cooling load or can be exerted for heat load for a local area called CHP/CCHP (Nasrabadi et al., 2022a; Abbasi et al., 2018; You et al., 2020a). Besides, Moghimi et al. (2018) evaluated a new Combined Cooling, Heat and Power (CCHP) configuration that includes a Rankine cycle, a Brayton cycle, a domestic water heater, and an ejector refrigeration cycle. The 4E analysis is utilized to assess performance, environmental impact and cost-effectiveness of the cycle compared to the simple Brayton cycle. Major design variables like pressure ratio of compressor, inlet temperature of turbine, pinch point temperatures, HRSG pressures, and regenerator effectiveness are studied to optimize the CCHP system by defining two different objectives, i.e., exergy efficiency and levelized total annual cost. Results show that the system has higher exergy and energy efficiencies of 7% and 12% than the corresponding Brayton unit, respectively. Likewise, A. E. Alali et al. (2022) examined a cogeneration scheme consisting of a Stirling engine, Double Effect absorption chiller, and Gas Turbine-Modular Helium Reactor scheme. The heat-based energy rejected from the Gas Turbine cycle utilized by the absorption cycle and Stirling engine to generate coolant and extra electricity, respectively. Results show that integrating these two units with the Gas Turbine-Modular Helium Reactor rises energy utilization efficiency by up to 5.5%-points at an inlet temperature of turbine range of 900 ∘C, while reduces the helium mass flow rate by up to 17.8%. In another case, Nianci Lu et al. (2020) studied on suppressing water level fluctuations in transient conditions of switching of a known steam turbine in China, using a dynamic simulation and identifying influential factors such as the flow rate of water circulated within the heating network.

There are many examples of using heat exchangers in industry to deliver heat loss from one system to another nearby system in order for using the maximum amount of energy. One of these examples is using temperature difference between the top and bottom level of sea water called Ocean Thermal Energy Conversion (OTEC). P. Ahmadi et al. (2013) conducted a study including OTEC system, joined to solar-boosted PEM electrolyzer, produces 1.2 kg/h of hydrogen with an exergetic efficiency of about 56.5%, while exergetic and energetic efficiencies of OTEC-based arrangement are 22.7% and 3.6%, correspondingly. In case of multi-generation systems driven by renewable energy, A. M. Nasrabadi and Korpeh (2023) analyzed a multi-generation scheme relying on wind and solar energies for electricity, freshwater, and hydrogen generation, with optimization leading to enhanced exergetic performance and reduced total cost rate, identifying a proposed region in Hormozgan province, Iran for building the power plant. Additionally, A combined scheme based on ocean thermal, wind, and solar energy sources was configured by J. R. Mehrenjani et al. (2022a) for power generation and hydrogen production, with a techno-economic model to calculate cost rate, exergetic efficiency, and generation capacity of hydrogen; multi-criteria optimization using genetic algorithm was considered to identify the most effective parameters on system performance, resulting in an increase in the exergetic efficiency of almost 19%. Emadi and Mahmoudimehr (2019) addressed a re-gasification cycle of LNG as a heat sink for a geothermal-based poly-generation arrangement. This scheme includes two ORCs, a PEM electrolyzer, and an absorption refrigeration cycle, and is analyzed both thermodynamically and economically. A multi-criteria optimization procedure is developed to identify the optimal exergetic efficiency, total cost rate, and generation rate of hydrogen, resulting in a design with significant improvements compared to existing literature. In this regard, J. R. Mehrenjani et al. (2022b) designed an integrated system that utilizes LNG as heat sink and a geothermal resources for producing hydrogen and its liquefaction, electric power, and coolant. The system is analyzed from both cost and thermodynamic perspectives, and a multi-objective optimization process is conducted to find the optimal total cost rate, hydrogen generation capacity, and exergetic efficiency, resulting in optimum values of 291.4 $/h, 154.9 kg/h, and 23.3%, respectively.

As discussed, Hydrogen could either be produced using renewable energy (Nasrabadi and Korpeh, 2023; Mehrenjani et al., 2022a; Yilmaz et al., 2020; Yilmaz and Ozturk, 2022) or non-renewable energy sources. Through a case study, Y. Cao et al. (2021) proposed a geothermal-based poly-generation scheme that consists of different cycles and units utilizing four various environmentally friendly fluids, and the best one is selected based on the 3E analysis. The results show that R123/R1234ze (e) offers the most suitable coolant, hydrogen, and freshwater generation rates, as well as energetic performance, while R600/R1234yf shows the lowest products' unit cost. Furthermore, M. Delpisheh et al. (2021) investigated a novel setup that uses parabolic trough solar collectors to simultaneously produce desalinated water and hydrogen in three solar radiation approaches, with electricity generated by an ORC; a sensitivity study is conducted to optimize the design state, with results showing different desalination rates and hydrogen production rates in different radiation approaches. A combined electricity, hydrogen, and natural gas scheme was suggested by V. Mehdikhani et al. (2022) that utilizes two geothermal wells with a novel flash configuration, ORC, LNG, and PEM systems, which was optimized through simulation using Engineering Equation Solver (EES) and achieved improved thermal efficiency and other values compared to similar studies. A novel configuration utilizing a parabolic collector field, PEM electrolyzer, and fuel cell for green hydrogen production during peak demand was also proposed, analyzed using thermodynamic and exergo-economic perspectives, and optimized through a sensitivity investigation and multi-criteria optimization revealing Dowtherm™ A as the best working fluid with cost rate of 492.4 $/h as well as exergetic efficiency of 17.6% by A. Razmi et. al (Razmi et al., 2022). Besides, Ates and Ozcan (2022) investigated Turkey's industrial waste heat potential, identifying feasible hydrogen and electricity conversion tools to yield valuable energy while electrochemical and thermochemical hydrogen production are utilized; the study finds that the minimum cost of hydrogen production task is related to the GT-HyS scheme, which has the potential to reduce CO_2 emissions by more than 720,000 ton/year.

Optimization process is an approach to find the best performance of a function called objective. In the field of energy, the energy systems are expected to work in optimum situation; so, applying an optimization algorithm is required. There are lots of thermo-economic and environmental analyses along with optimization process in the literature (Moghimi et al., 2018; Nasrabadi and Korpeh, 2023; Pourrahmani and

Moghimi, 2019). In some cases, the optimization process is very time-consuming and needs to be reduced. One of the new approaches to reduce the run-time of optimization process is training a neural network and then generate a function using the trained network instead of a non-linear mathematical function. Neural networks have the ability to learn complex patterns and relationships in energy systems data, enabling them to predict system behavior with high accuracy. By analyzing historical data, neural networks can forecast energy demand, optimize energy generation, and improve overall system efficiency, leading to more informed decision-making and better resource allocation. Optimization process can be reduced by using machine learning (neural network) models and some examples could be found in literature (Nasrabadi et al., 2022a; Nasrabadi and Moghimi, 2022; Haghghi et al., 2023a).

1.2. Contributions

As mentioned, some researchers have addressed multi-generation systems effectively, but they have not tackled a fully-recovered energy system with a comprehensive analysis. There is a gap in the literature where a well-designed and fully-recovered system, incorporating CCHP, hydrogen production, and LNG, should be proposed with consideration of in-depth techno-economic and environmental analysis. To address these shortcomings, the authors of this study aim to propose a system that maximizes heat recovery, facilitates multi-production, and utilizes LNG. The combination of LNG with ORCs enhances power generation capabilities by capturing and utilizing waste heat that would otherwise go unused. This leads to a more efficient and effective power generation process. Additionally, ORC systems can be specifically designed to operate on low-temperature heat sources like exhaust gas, making them a suitable companion for LNG. As a result, integrating ORCs with LNG shows promise in improving energy efficiency and harnessing more power from available resources. Furthermore, heat recovery in gas turbine-based power plants can be combined with absorption chiller refrigerators to create a more efficient and sustainable energy system. By capturing waste heat from gas turbine exhaust, absorption chillers can convert it into useful cooling power for air conditioning or refrigeration purposes. This process reduces waste heat released into the environment, while also providing cost savings and lower carbon emissions. Overall, the combination of heat recovery and absorption chiller refrigeration technology offers a promising approach to enhancing the sustainability and efficiency of power generation systems. One of the key benefits of the proposed system is producing hydrogen from generated power using a PEM electrolyzer, making it a promising energy resource for the near future. Lastly, the entire system is mathematically modeled and calculated using MATLAB programming code. The objectives of the model are optimized using a Genetic Algorithm (GA) and a machine learning model to reduce runtime. These characteristics make the present study unique and distinguish it from similar works. To highlight the most important goals of the present study, the following points are classified:

- Researchers have addressed multi-generation systems but not a fully-recovered energy system with comprehensive analysis.
- The authors aim to propose a system with maximum heat recovery, multi-production, and LNG utilization.
- Combining LNG with ORCs increases power generation capabilities by capturing and utilizing waste heat.
- ORC systems operating on low-temperature heat sources like exhaust gas are compatible with LNG.
- Integrating heat recovery with absorption chiller refrigerators improves energy efficiency and sustainability.
- By capturing waste heat, absorption chillers convert it into useful cooling power for air conditioning or refrigeration.
- The proposed system benefits from producing hydrogen from generated power using a PEM electrolyzer.
- The entire system is mathematically modeled and optimized using a MATLAB programming code and Genetic Algorithm (GA) for efficiency.

2. System description

The system proposed in the current study includes a gas turbine integrated with an SRC, two cascaded ORCs, an Absorption Refrigeration Cycle (ARC), an LNG expander, and a PEM electrolyzer for generating more power, producing a cooling load, and producing hydrogen simultaneously.

Fig. 1 shows a schematic of the system, presenting and clarifying the numbered steps, components, and subsystems. In the gas turbine, air enters the compressor and exits at a much higher pressure. The pressurized air and fuel are then burned in the combustion chamber to produce a large amount of energy. The exhaust gas from this process enters the turbine to generate power. Afterward, the exhausted gas flows into evaporators 1 and 2, transferring its heat to an SRC and ORC. The heat loss in the SRC can still be recovered and delivered to an ARC to produce a cooling load. To enhance the system's efficiency further, a heat recovery unit in the ORC can operate another ORC, with its condenser being cooled by an LNG stream. The LNG stream, a high-pressure and low-temperature liquid natural gas, can be used to deliver cooling load to a nearby area and can also be expanded through a turbine to generate additional power before being used as a fuel. The LNG then undergoes a phase change from liquid to gas and is delivered to the domestic sector through pipelines. The operating fluids in the SRC, first ORC, ARC, and second ORC are water, R134a, two-phase ammonia-water, and ethane, respectively. Liquid-phase water is pressurized by a water pump and then heated through evaporator 1 to vaporize and enter the SRC's turbine. After power generation, the steam still retains heat and transfers it to the ARC through the SRC's condenser (8−9−10−11). R134a, in liquid form, passes through a pump and gains sufficient thermal energy to become steam, which operates a turbine to generate electricity. The heat generated in condenser 2 can be utilized to operate another ORC with ethane as the working fluid. This ORC is cooled by LNG and generates additional power. Part of the produced electric power is directed to a PEM electrolyzer to separate oxygen and hydrogen from pure water. These products are stored in storage tanks for transportation and use in medical applications and fuel utilization, respectively.

3. Mathematical methodology

This chapter introduces the thermo-economic and environmental equations utilized to model the suggested arrangement. In addition, some assumptions were made to simplify the system modeling. These are listed below:

- All components in the system operate under stable conditions.All components in the system operate under stable conditions.
- Reductions in pressure along pipelines and interconnections are not taken into account.
- Changes in potential and kinetic terms are excluded from energy and exergy analyses.
- The dead state features are set at 25 °C and 101 kPa.

3.1. First law analysis

The first law of thermodynamics is the principle of energy conservation, stating that energy cannot be created or destroyed but can only change forms. Understanding and applying this law is crucial for analyzing energy systems as it enables accurate assessment and optimization of energy use and efficiency. The first law of thermodynamics is applied to derive mass and energy balance equations for each

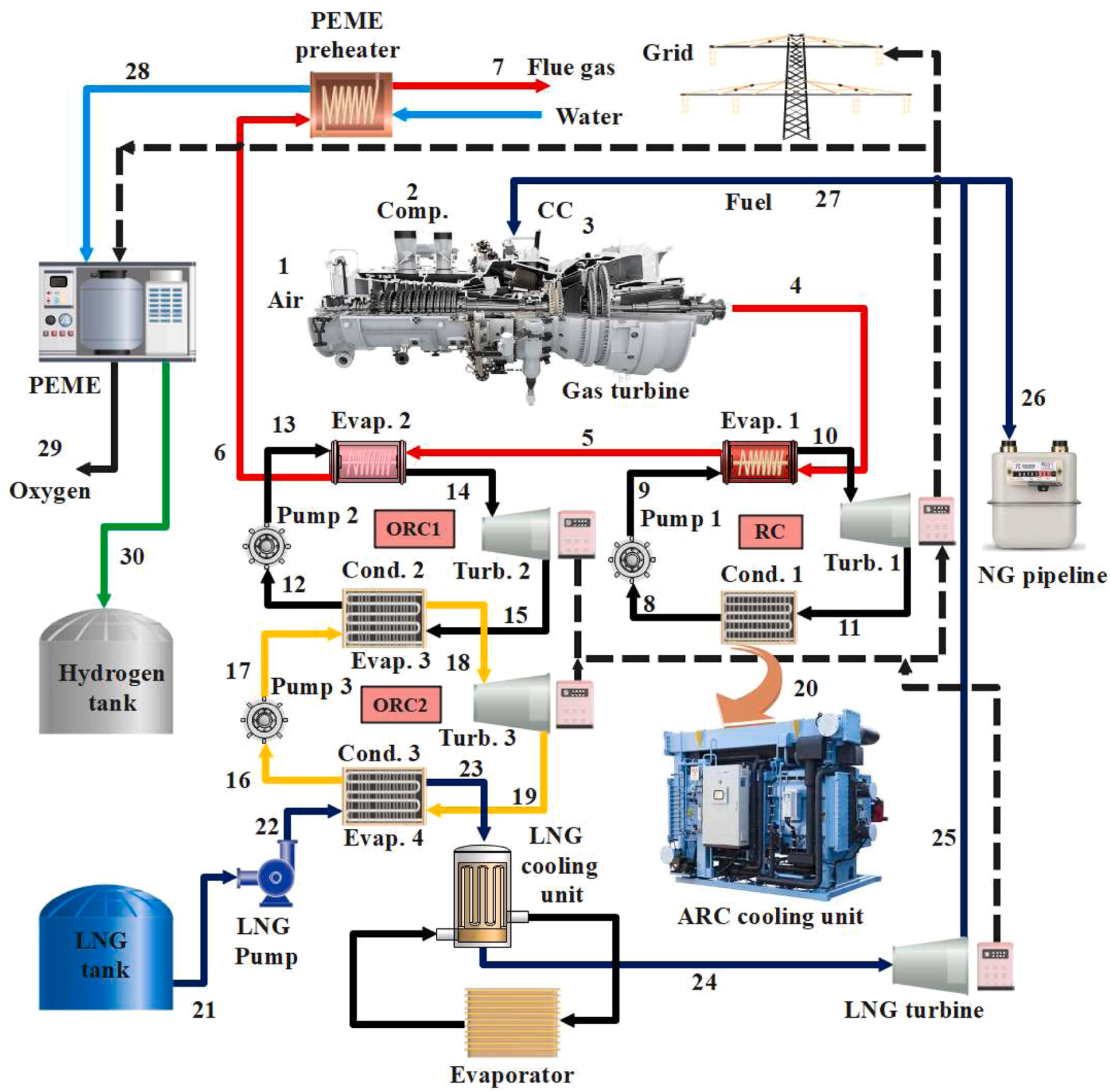

Fig. 1. Schematic of the proposed system.

component in the system, assuming negligible changes in kinetic and potential energy (Wang et al., 2023; Xia et al., 2022).

$$\Sigma\dot{m}_{in} = \Sigma\dot{m}_{out} \tag{1}$$

$$\dot{Q} - \dot{W} \quad \sum\left(\dot{m}h\right)_{out} - \sum(\dot{m}h)_{in} \tag{2}$$

The flow enthalpy, denoted by h, is indicated by the subscripts "out" and "in" which correspond to exit and entrance states.

Table 1 provides the energy equations for the established devices of power cycles.

In this study, correlations provided by Pátek and Klomfar (2006) are considered to calculate the thermodynamic properties of Li-Br/water mixtures.

- Liquefied natural gas (LNG) regasificationLiquefied natural gas (LNG) regasification

Liquefied natural gas (LNG) regasification is a significant process that involves the conversion of LNG into its gaseous form to be utilized as fuel. This intricate procedure encompasses various sequential stages, including unloading, storage, pre-treatment, regasification, gas processing, and distribution. Initially, the LNG is discharged from the

Table 1
Equations that account for the balance of energy in various components within SRC and ORCs (Nasrabadi et al., 2022a; Abbasi et al., 2018; Khanmohammadi et al., 2017; Li et al., 2023; Miao et al., 2021).

Component	Equation
SRC:	
Turbine	$\dot{W}_{T,RC} = \dot{m}_{RC}(h_{10} - h_{11}),\ \eta_{T,RC} = (h_{10} - h_{11})/(h_{10} - h_{11,is})$
Evaporator	$\dot{Q}_{Eva,RC} = \dot{m}_{RC}(h_{10} - h_9) = \dot{m}_{Flue}(h_4 - h_5)$
Pump	$\dot{W}_{P,RC} = \dot{m}_{RC}(h_9 - h_8),\ \eta_{P,RC} = (h_{9,is} - h_8)/(h_9 - h_8)$
Condenser	$\dot{Q}_{Con,RC} = \dot{m}_{RC}(h_{11} - h_8) = \dot{Q}_{Gen,ARC}$
ORC 1:	
Turbine	$\dot{W}_{T,ORC1} = \dot{m}_{ORC1}(h_{14} - h_{15}),\ \eta_{T,ORC1} = (h_{14} - h_{15})/(h_{14} - h_{15,is})$
Evaporator	$\dot{Q}_{Eva,ORC1} = \dot{m}_{ORC1}(h_{14} - h_{13}) = \dot{m}_{Flue}(h_5 - h_6)$
Pump	$\dot{W}_{P,ORC1} = \dot{m}_{ORC1}(h_{13} - h_{12}),\ \eta_{P,ORC1} = (h_{13,is} - h_{12})/(h_{13} - h_{12})$
Condenser	$\dot{Q}_{Con,ORC1} = \dot{m}_{ORC1}(h_{15} - h_{12}) = \dot{m}_{ORC2}(h_{18} - h_{17})$
ORC2:	
Turbine	$\dot{W}_{T,ORC2} = \dot{m}_{ORC2}(h_{18} - h_{19}),\ \eta_{T,ORC2} = (h_{18} - h_{19})/(h_{18} - h_{19,is})$
Evaporator	$\dot{Q}_{Eva,ORC2} = \dot{m}_{ORC2}(h_{18} - h_{17}) = \dot{m}_{ORC1}(h_{15} - h_{12})$
Pump	$\dot{W}_{P,ORC2} = \dot{m}_{ORC2}(h_{17} - h_{16}),\ \eta_{P,ORC2} = (h_{17,is} - h_{16})/(h_{17} - h_{16})$
Condenser	$\dot{Q}_{Con,ORC2} = \dot{m}_{ORC2}(h_{19} - h_{16}) = \dot{m}_{LNG}(h_{23} - h_{22})$

carrier vessel and securely stored in insulated tanks until required for usage. The pre-treatment phase entails the application of waste heat to elevate the temperature of the LNG, followed by further heating using warm water or steam until it reaches its boiling point. This causes the LNG to undergo vaporization and expand into a gaseous state. Subsequently, gas processing is conducted to eliminate impurities from the gas before it is distributed through pipelines or transported via trucks to end-users. Therefore, LNG regasification assumes a pivotal role in facilitating the utilization of natural gas as an efficient and adaptable energy source. Moreover, the liquefaction of natural gas serves as a means to reduce transportation costs by significantly decreasing its volume. This study presents a novel integration of organic Rankine cycles (ORCs) and liquefied natural gas (LNG) regasification processes for the simultaneous generation of electricity, cooling, and hydrogen. This innovative approach offers multiple advantages, including enhanced system performance and efficient utilization of waste heat. By employing LNG as a thermal reservoir for ORCs, the conversion of low-quality waste heat into valuable energy is facilitated, ensuring reliable operation during periods of geothermal resource unavailability. LNG is typically considered as a real gas due to its behavior at high pressures and low temperatures. Real gases deviate from ideal gas behavior, especially when subjected to conditions where intermolecular forces and molecular volume become significant. To compute the properties of LNG, including thermodynamic and transport properties, software packages like REFPROP can be utilized. REFPROP is a widely used program that provides accurate thermophysical properties for various substances, including LNG. REFPROP employs equations of state, such as the Peng-Robinson or Redlich-Kwong equations, along with other specialized models to calculate the properties of real gases, considering factors like pressure, temperature, composition, and phase behavior. It incorporates extensive experimental data and correlations to ensure accurate calculations. Table 2 presents the related relations for the LNG stream.

- Proton exchange membrane (PEM) electrolysisProton exchange membrane (PEM) electrolysis

Proton exchange membrane (PEM) electrolysis is a process that uses an electrolytic cell to split water into hydrogen and oxygen using an external power source. The process involves passing an electric current through a proton exchange membrane to separate the positively charged hydrogen ions from the negatively charged oxygen ions. The hydrogen ions then combine to form hydrogen gas, while the oxygen ions form oxygen gas. This process is a key method of producing hydrogen gas for use in fuel cells and other applications.

Table 3 lists and provides brief descriptions of the governing equations for the PEM electrolyzer (Liu et al., 2023; Sun et al., 2023a, 2023b).

3.2. Exergy analysis

Exergy account is a thermodynamic method considered to study the quality of energy in a system and to identify inefficiencies and losses. By quantifying the amount of work that can be obtained from energy, it provides insights into opportunities for improving energy efficiency and reducing waste, making it a valuable tool for optimizing energy systems.

Table 2
Equations that depict the balance of energy for different parts of the liquefied natural gas (LNG) stream (Emadi and Mahmoudimehr, 2019; Mehrenjani et al., 2022b; Chitgar and Moghimi, 2020).

Component	Equation
LNG pump	$\dot{W}_{P,LNG} = \dot{m}_{LNG}(h_{22} - h_{21}),\ \eta_{P,LNG} = (h_{22,is} - h_{21})/(h_{22} - h_{21})$
LNG evaporator	$\dot{Q}_{Vap,LNG} = \dot{m}_{LNG}(h_{23} - h_{22}) = \dot{m}_{ORC2}(h_{19} - h_{16})$
Domestic cooling unit	$\dot{Q}_{DCU} = \dot{m}_{LNG}(h_{23} - h_{24})$
LNG turbine	$\dot{W}_{T,LNG} = \dot{m}_{LNG}(h_{24} - h_{25}),\ \eta_{T,LNG} = (h_{24} - h_{25})/(h_{24} - h_{25,is})$

Table 3
Governing equations of the PEME (Mehrenjani et al., 2022a; Zuo et al., 2023).

Parameter	Governing equations
Required energy for reaction	$\Delta H = \Delta G + T\Delta S$
Input power	$E_{elec} = Q_{elec} = JV$
Overpotential of the cell	$V = V_0 + V_{ohm} + V_{activ,a} + V_{activ,c}$
Nernst voltage	$V_0 = 1.229 - 8.5\times10^{-4}(T_{PEM} - 298)$
Ohmic overpotential	$V_{ohm} = JR_{PEM}$
Activation overpotential	$V_{activ,i} = \frac{RT}{F}\sinh^{-1}\left(\frac{J}{2J_{0,i}}\right)\ i = a,c$
Exchange current density	$J_{0,i} = J_i^{ref}\exp\left(-\frac{E_{activ,i}}{RT}\right)\ i = a,c$
Overall ohmic resistance	$R_{PEM} = \int_0^D \frac{dx}{\sigma[\lambda(x)]}$
Local ionic conductivity	$\sigma[\lambda(x)] = [0.5139\lambda(x) - 0.326]\exp\left[1268\left(\frac{1}{303} - \frac{1}{T}\right)\right]$
Water content at a location x	$\lambda(x) = \frac{\lambda_a - \lambda_c}{D}x + \lambda_c$

The exergy account can be provided as (Bejan et al., 1995):

$$\dot{E}x_Q + \sum_i \dot{m}_i ex_i = \sum_e \dot{m}_e ex_e + \dot{E}x_W + \dot{E}x_d \tag{3}$$

where i and e stand for inlet and exit, respectively.

$$ex_{ph} = h - h_0 - T_0(s - s_0) \tag{4}$$

$$\dot{E}x_Q = \left(1 - \frac{T_0}{T}\right)\dot{Q} \tag{5}$$

$$\dot{E}x_W = \dot{W} \tag{6}$$

where ex_{ph}, $\dot{E}x_Q$ and $\dot{E}x_W$ is physical exergy, exergy of heat, and work exergy, respectively.

Table 4 displays the equations that illustrate the destructed exergy for each component of the scheme. Additionally, the system's exergetic efficiency is calculable based on the following equation, which provides a measure of how effectively the system is able to convert input energy into useful work.

$$\varepsilon_{system} = \frac{\dot{E}x_{Electricity} + \dot{E}x_{Hydrogen} + \dot{E}x_{Cooling}}{\dot{E}x_{Fuel} + \dot{E}x_{LNG}} \tag{7}$$

3.3. Economic and environmental analysis

Economic assessment is used to assess the financial feasibility of energy systems. It helps to identify the most cost-effective solutions for achieving energy goals and minimizing investment risks, making it an important consideration when designing and implementing energy projects. By assessing the economic viability of different options, it enables informed decision-making for optimizing energy systems. In order to obtain a complete economic assessment of the integrated system, it is possible to predict the cost rates of components based on investment costs outlined in Table 5. Additionally, the capital recovery factor (CRF) can be calculated using the Eq. (8) (You et al., 2020b; Bamisile et al., 2023):

$$CRF = \frac{i(1+i)^N}{(1+i)^N - 1} \tag{8}$$

The cost indexes are employed to update reference cost functions to the current year. This can be observed in the following formulation (Emadi and Mahmoudimehr, 2019):

$$Z_{Current\quad year} = Z\frac{CI_{Current\quad year}}{CI_{reference}} \tag{9}$$

The mean cost index for the year 2022, with a value of 816, is utilized to revise and adjust the equipment expenses in the existing modeling

Table 4
Exergy balance relations for main components (Nasrabadi et al., 2022a; Mehrenjani et al., 2022b).

Component	Rate of exergy destruction
Gas turbine cycle	
Compressor	$\dot{E}x_{D,Comp} = \dot{E}x_{CS} - \dot{E}x_{CD} + \dot{W}_{Comp}$
Combustion chamber	$\dot{E}x_{D,CC} = \dot{E}x_{CD} - \dot{E}x_{TI} + \dot{m}_{fuel}ex^0_{ch,fuel}$
Gas turbine	$\dot{E}x_{D,GT} = \dot{E}x_{TI} - \dot{E}x_{TE} - \dot{W}_{GT}$
Rankine Cycle	
Turbine	$\dot{E}x_{D,T,RC} = \dot{E}x_{10} - \dot{E}x_{11} - \dot{W}_{T,RC}$
Evaporator	$\dot{E}x_{D,Eva,RC} = \dot{E}x_9 + \dot{E}x_4 - \dot{E}x_5 - \dot{E}x_{10}$
Pump	$\dot{E}x_{D,P,RC} = \dot{E}x_8 - \dot{E}x_9 + \dot{W}_{P,ORC1}$
Condenser	$\dot{E}x_{D,Con,RC} = \dot{E}x_{11} - \dot{E}x_8 + \dot{Q}_{Gen}$
Organic Rankine Cycle 1	
Turbine	$\dot{E}x_{D,T,ORC1} = \dot{E}x_4 - \dot{E}x_{15} - \dot{W}_{T,ORC1}$
Evaporator	$\dot{E}x_{D,Eva,ORC1} = \dot{E}x_{15} + \dot{E}x_{17} - \dot{E}x_{12} - \dot{E}x_{18}$
Pump	$\dot{E}x_{D,P,ORC1} = \dot{E}x_{12} - \dot{E}x_{13} + \dot{W}_{P,ORC1}$
Condenser	$\dot{E}x_{D,Con,ORC1} = \dot{E}x_{15} + \dot{E}x_{17} - \dot{E}x_{12} - \dot{E}x_{18}$
Organic Rankine Cycle 2	
Turbine	$\dot{E}x_{D,T,ORC2} = \dot{E}x_{18} - \dot{E}x_{19} - \dot{W}_{T,ORC2}$
Evaporator	$\dot{E}x_{D,Eva,ORC2} = \dot{E}x_{15} + \dot{E}x_{17} - \dot{E}x_{12} - \dot{E}x_{18}$
Pump	$\dot{E}x_{D,P,ORC2} = \dot{E}x_{16} - \dot{E}x_{17} + \dot{W}_{P,ORC2}$
Condenser	$\dot{E}x_{D,Con,ORC2} = \dot{E}x_{19} + \dot{E}x_{22} - \dot{E}x_{16} - \dot{E}x_{23}$
LNG stream	
LNG pump	$\dot{E}x_{D,P,LNG} = \dot{E}x_{21} - \dot{E}x_{22} + \dot{W}_{P,LNG}$
LNG evaporator	$\dot{E}x_{D,Vap,LNG} = \dot{E}x_{19} + \dot{E}x_{22} - \dot{E}x_{16} - \dot{E}x_{23}$
Domestic cooling unit	$\dot{E}x_{D,DCU,LNG} = \dot{E}x_{23} - \dot{E}x_{24} + \dot{Q}_{DCU}$
LNG turbine	$\dot{E}x_{D,T,LNG} = \dot{E}x_{24} - \dot{E}x_{25} - \dot{W}_{T,LNG}$
Absorption refrigeration cycle	
Absorber	$\dot{E}x_{D,Abs} = \dot{E}x_{WS} + \dot{E}x_R - \dot{E}x_{SS}$
ARC condenser	$\dot{E}x_{D,ARC,cond} = Q_{ARC,Cond} + \dot{E}x_{ARC,Cond,in} - \dot{E}x_{ARC,Cond,out}$
ARC evaporator	$\dot{E}x_{D,ARC,Eva} = \dot{E}x_{Q_{Eva}} + \dot{E}x_{ARC,Eva,in} - \dot{E}x_{ARC,Eva,out}$
Solution pump	$\dot{E}x_{D,SP} = \dot{W}_{SP} + \dot{E}x_{ARC,SP,in} - \dot{E}x_{ARC,SP,out}$
Solution expansion valve	$\dot{E}x_{D,SEV} = \dot{E}x_{ARC,SEV,in} - \dot{E}x_{ARC,SEV,out}$
Refrigerant expansion valve	$\dot{E}x_{D,REV} = \dot{E}x_{ARC,REV,in} - \dot{E}x_{ARC,REV,out}$
PEM Electrolyzer	$\dot{E}x_{D,Elec} = \dot{E}x_{28} - \dot{E}x_{29} - \dot{E}x_{30} + \dot{W}_{Elec}$

framework. Furthermore, it is possible to define the overall cost rate of the system using the following calculation (Emadi and Mahmoudimehr, 2019):

$$\dot{Z}_{tot} = \frac{CRF \times \varphi \times \sum_k Z_k}{t_{hour}} \tag{10}$$

The equations of each cost function are provided through Table 5 and the utilized values in the cost assessment are presented in Table 6.

The total cost rate of the arrangement is the sum of the cost rate for all equipment involved in the process, such as pumps, heat exchangers, and turbines, as well as the fuel cost rate required to operate the system (Moghimi et al., 2018), (Nasrabadi et al., 2022b).

$$\dot{C}_f = c_f \times \dot{m}_{fuel} \times 3600 \tag{11}$$

$$\dot{C}_{\text{total, cost}} = \sum_k \dot{Z}_k + \dot{C}_f + \dot{C}_{env} \tag{12}$$

where $\dot{m}_{fuel}$ is the fuel mass flow rate and c_f is the price of fuel per unit of mass ($/kg).

To assess the economic advantage of producing varying products, such as electricity and hydrogen, the levelized cost can be applied. This is achieved by calculating the levelized cost for each product based on its production capacity and the associated costs of the relevant units, using the following equations (Mehrenjani et al., 2022b; Bamisile et al., 2023; Abbasi and Pourrahmani, 2020; Behnam et al., 2018; Haghghi et al., 2023b):

$$LCOE = \frac{\dot{Z}_{GT} + \dot{Z}_{RC} + \dot{Z}_{ORC}}{\dot{W}_{net,total}} \tag{13}$$

$$LCOH = \frac{(LCOE \times \dot{W}_{Elec}) + \dot{Z}_{PEME}}{\dot{m}_{H_2}} \tag{14}$$

where $\dot{W}_{Elec}$ represents the amount of input electricity of the electrolyzer.

The CO_2 emission rate is expressed according to the following equations which is defined as an economical function (You et al., 2020a; Moghimi et al., 2018; Tahir et al., 2021; Wang et al., 2022; Liu et al., 2022a):

$$m_{CO_2} = \frac{0.15E16\tau^{0.5}\exp\left(-71100/T_{pz}\right)}{P_3^{0.05}(\Delta P_{cc}/P_3)^{0.5}} \tag{15}$$

$$\dot{C}_{env} = c_{CO_2} \times m_{CO_2} \times 3600 \tag{16}$$

where, c_{CO_2} is penalty per unit of CO_2 production in the gas turbine's combustion chamber and is equal to 0.024 $/kg. m_{CO_2} is rate of CO_2 emission (kg/s) and 3600 is for unit convert from dollar per seconds into dollar per hour. τ is combustion residence time (0.002 s) and T_{pz} is the maximum temperature in the combustion chamber. ΔP_{cc} represents pressure drop in combustion chamber (Liu et al., 2022b).

4. Optimization procedure

It is clear that the use of MATLAB programming code to calculate model functions can be a time-consuming process when optimizing the model functions. This is due to the fact that the computation time for each generation would have to be multiplied by the number of generations and populations, resulting in a significant amount of time being spent on calculations. To overcome this issue, an artificial neural network (ANN) model has been introduced as a replacement for the MATLAB function. The ANN model significantly reduces run time and can optimize model functions effectively. Table 7 outlines the various parameters and considerations related to the implementation of the ANN model. With the implementation of the ANN model, researchers and scientists can save significant amounts of time while still obtaining accurate results when optimizing model functions.

In the current research, a variety of objective functions were evaluated to optimize the overall system. These included the energy efficiency of the entire scheme, the total cost rate, and the rate of hydrogen production. To achieve this optimization, Genetic Algorithms (GA) were employed, which allowed the team to locate optimum points in the final generation. To designate the final optimum solution for the three objective functions, LINMAP was utilized. This involves using normalized values of the objectives to calculate the optimum solution. Normalization involves scaling the objective functions to a common range to make them comparable. The calculation of optimum points was carried out using this normalization method, which allows for easy comparison and evaluation of results. Overall, this approach provides an effective and efficient means of optimizing the system and identifying key areas for improvement (Mehrenjani et al., 2022a; Chitgar and Moghimi, 2020).

$$f^{\star}_{i,j} = \frac{f_{i,j}}{\sqrt{\sum_{i=1}^{N} \left(f_{i,j}\right)^2}}, j = 1, 2, 3 \tag{17}$$

$$d_i = \sqrt{\sum_{j=1}^{3} \left(f^*_{i,j} - f^*_{\text{ideal},j}\right)^2} \tag{18}$$

where $f^{\star}_{i,j}$ is normalized values of objective functions; $f^*_{\text{ideal},j}$ represents ideal point for each objective function, and d_i finds the least distance of optimum values with the ideal points of all objective functions (Bamisile et al., 2023; Shakibi et al., 2023). The characteristics and parameters of

Table 5
Cost functions of each component (Mehrenjani et al., 2022b; Alirahmi et al., 2021; Mehrpooya et al., 2021; Zang et al., 2018).

	Component	Cost Function	Reference Year	CEPCI
PEM	Electrolyzer	$Z_{elec} = 1000 \times \dot{W}_{elec}$	2018	603.1
	Preheater	$Z_{Pre} = 130\left(\frac{A_{Pre}}{0.093}\right)^{0.78}$	2005	468
Gas turbine cycle	Compressor	$Z_{AC} = \left(\frac{39.5\dot{m}_a}{0.9-\eta_{AC}}\right)\left(\frac{P_2}{P_1}\right)\mathrm{Ln}\left(\frac{P_2}{P_1}\right)$	1994	368.1
	Combustion chamber	$Z_{CC} = \left(\frac{25.6\dot{m}_a}{0.995-\frac{P_6}{P_4}}\right)[1+\exp(0.018T_4-26.4)]$	1994	368.1
	Gas turbine	$Z_{GT} = \left(\frac{266.3\dot{m}_g}{0.92-\eta_{GT}}\right)Ln\left(\frac{P_6}{P_7}\right)[1+\exp(0.036T_4-54.4)]$	1994	368.1
Steam Rankine cycle (SRC)	Evaporator	$Z_{Eva,ORC} = 309.14(A_{Eva})^{0.85}$	2001	394
	Turbine	$Z_{T,ORC} = 4750\left(\dot{W}_T\right)^{0.75}$	2001	394
	Pump	$Z_{P,ORC} = 200\left(\dot{W}_P\right)^{0.65}$	2001	394
	Condenser	$Z_{Con,ORC} = 516.62(A_{Con})^{0.6}$	2001	394
Organic Rankine cycles (ORCs)	Evaporator	$Z_{Eva,ORC} = 309.14(A_{Eva})^{0.85}$	2001	394
	Turbine	$Z_{T,ORC} = 4750\left(\dot{W}_T\right)^{0.75}$	2001	394
	Pump	$Z_{P,ORC} = 200\left(\dot{W}_P\right)^{0.65}$	2001	394
	Condenser	$Z_{Con,ORC} = 516.62(A_{Con})^{0.6}$	2001	394
LNG	Turbine	$Z_{T,LNG} = 4750\left(\dot{W}_T\right)^{0.75}$	2001	394
	Pump	$Z_{P,LNG} = 200\left(\dot{W}_P\right)^{0.65}$	2001	394
	Domestic Cooling Unit	$Z_{DCU} = 130\left(\frac{A_{CU}}{0.093}\right)^{0.78}$	2005	468
ARC	Generator	$Z_{Gen} = 17500\left(\frac{A_{Gen}}{100}\right)^{0.6}$	2000	394.1
	Reheater	$Z_{Reheater} = 8000\left(\frac{A_{Reheater}}{100}\right)^{0.6}$	2000	394.1
	Evaporator	$Z_{Evap} = 16000\left(\frac{A_{Evap}}{100}\right)^{0.6}$	2000	394.1
	Absorber	$Z_{Abs} = 16000\left(\frac{A_{Abs}}{100}\right)^{0.6}$	2000	394.1
	Solution HX	$Z_{SHX} = 12000\left(\frac{A_{SHX}}{100}\right)^{0.6}$	2000	394.1
	Solution pump	$Z_{S-P} = 2100\left(\frac{\dot{W}}{10}\right)^{0.26}\left(\frac{1-\eta_{S-P}}{\eta_{S-P}}\right)^{0.5}$	2000	394.1

Table 6
Values utilized in the economic analysis (Moghimi et al., 2018; Nasrabadi and Korpeh, 2023; Mehrenjani et al., 2022a).

Definition	Parameter	Value
System's lifetime	N	25 years
Rate of interest	I	12%
OM factor	Φ	1.06
Yearly working time	T	8000 h

Table 7
Parameters of the optimization method based on ANNs (Strušnik and Avsec, 2022).

Parameter	Values / Features
Number of iterations	5000
Number of data for training/test/ validation	700/150/150
Number of hidden layers/ hidden neurons	3/5
Validation checks	10
Initial weights and bias values	Random
Learning Rule	Levenberg-Marquardt Back Propagation
Transfer Function	Hidden: Log-Sigmoid, Output: Purelin

Table 8
Characteristics of the optimization algorithm (Strušnik and Avsec, 2022).

Parameter	Value
Mathematical Algorithm	Genetic Algorithm
Population Size	300
Maximum Generation	100
Number of Variables	5
Crossover Fraction	0.8
Function Tolerance	1e-4
Selection	Tournament

GA are presented in Table 8.

Parameters being used as input in the present model, their intervals of variation, and their units are listed in Table 9.

Fig. 2 shows schematic of the ANN model used for this study and how it works with the neurons and inputs and outputs data set.

Table 9
The range of variation of optimization variables.

Parameter	Lower bound	Upper bound
Fuel flow rate (kg/s)	100	200
Pressure ratio in air compressor (-)	6	18
SRC turbine1 inlet pressure (MPa)	1000	10,000
Heat exchanger effectiveness (-)	0.5	0.9
LNG pressure (MPa)	1000	3000

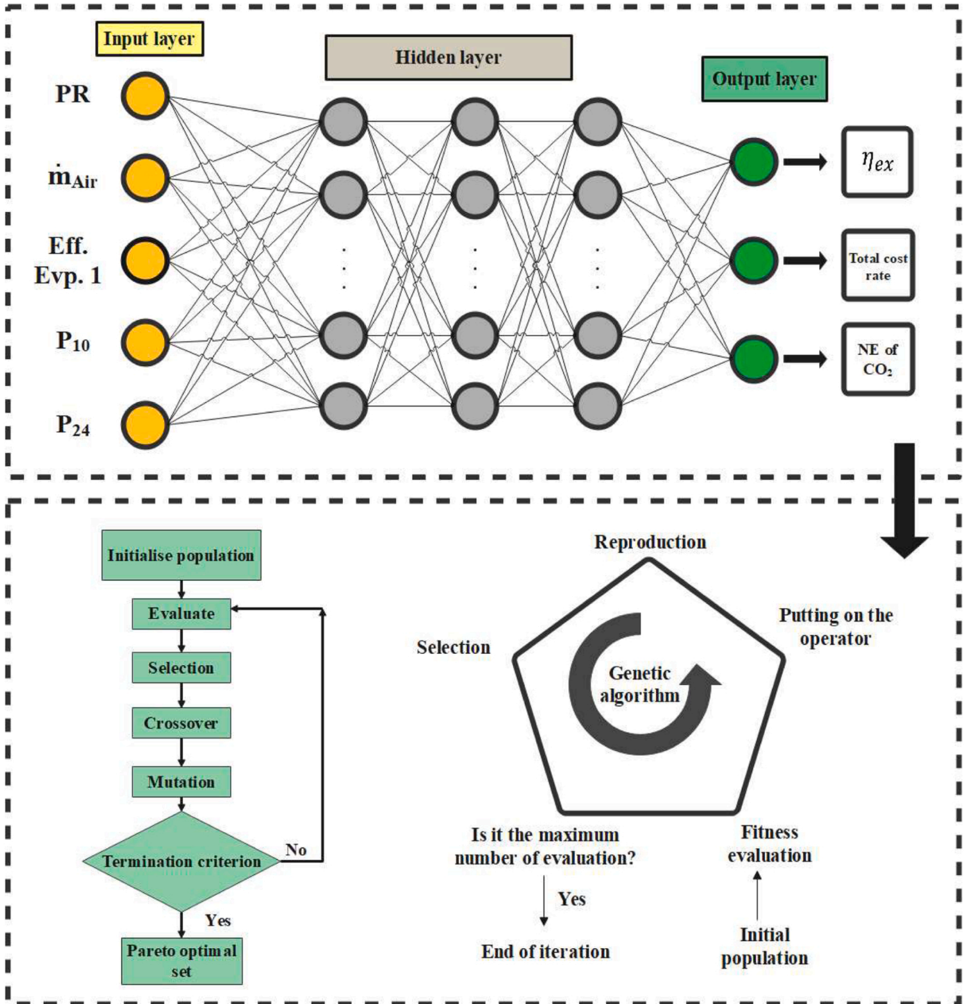

Fig. 2. Schematic of the ANN model and neurons.

5. Results and discussion

The process of obtaining outcomes from the mathematical model and programming code has been completed. The results have been analyzed and are presented in this section, where we explore the impact of different parameters on the key outputs of the model through a parametric study. This allows us to better understand how changes in various variables affect the overall performance of the model. Furthermore, an optimization process was carried out using a neural network algorithm. The results of this optimization process are also presented here. Through this process, we were able to further improve the performance of the model by identifying the optimal values for specific parameters. Overall, these findings provide valuable insights into the behavior of the model and its sensitivity to different input parameters. They can be used to guide future improvements and refinements to the model, as well as to inform decision-making processes based on the model's predictions.

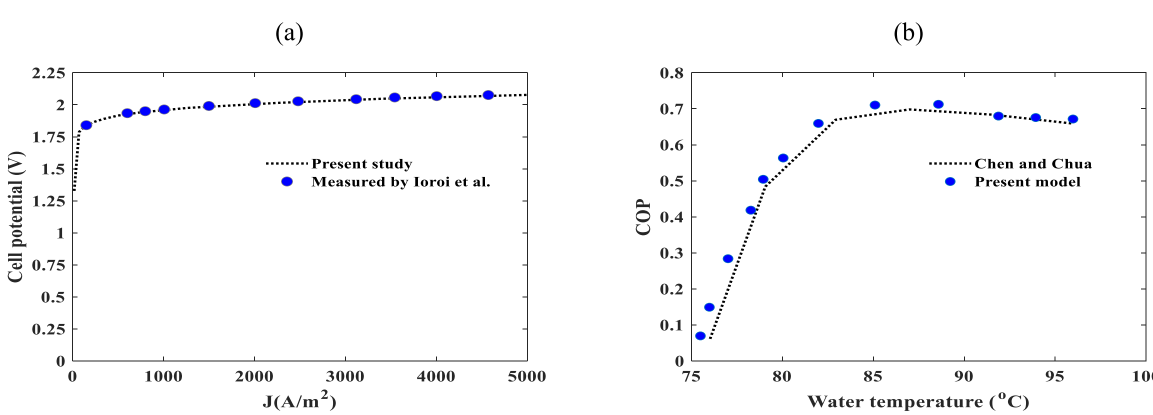

Fig. 3. Validation of PEM (a) and ARC (b).

5.1. Model verification

The outcomes of the arranged model being utilized in the current study is compared to similar studies, subsystem by subsystem, in order for verifying the MATLAB programming code. In Fig. 3(a) and (b) blue points represent the outcomes of the proposed model and dotted line shows the results from literature for PEME and ARC, respectively. Results revealed that the code for PEME and ARC are very reliable and can be used for the entire model calculations.

Subsystems ORCs, SRC, and GT validations are presented in Table 10. In this table, results of one of the ORCs represents the verification of other ORC and SRC because they are similar to each other with different working fluids. The LNG subsystem also has been verified according to Mosaffa et al. (2017) results as well. Validation of the LNG has been presented in Table 11.

Mean squared error (MSE) is a commonly used metric for evaluating the accuracy of artificial neural networks (ANNs). It measures the average squared difference between the predicted and actual values. A lower MSE indicates better accuracy. MSE is calculated by summing the squared differences between predicted and actual values, dividing by the number of samples, and taking the mean. It provides a quantitative measure of how well the ANN's predictions align with the true values. Results of ANN validation and how the model has been trained and the regression for each objective function have been provided through Fig. 4. The regressions are approximately 1 for all the objective functions which shows the machine learning algorithm has precisely been trained for the set of data.

5.2. Parametric study results

The process of analyzing the impact of each variable on a system's main outputs can be performed by conducting a parametric study. This involves isolating one parameter at a time while keeping all other variables constant in order to examine the specific role of each variable in the overall system. To conduct such an analysis, the main functions of the model are utilized to acquire and analyze results produced when various parameters are altered. Through careful examination of these results, trends and patterns can be identified, revealing important insights into the behavior of the system and its sensitivity to changes in different variables. A thorough parametric study can provide a deeper understanding of the complex relationships between variables and the system's main outputs, which can then be used to make more informed decisions and improve the performance of the system over time. Its importance lies in its ability to isolate the effects of individual variables, thereby providing valuable information for optimizing and refining the system.

The air mass flow rate is a crucial factor in determining the system's main outputs and is related to the inlet fuel in the gas turbine's combustion chamber through the equivalence ratio. As the inlet air in the compressor increases, the inlet fuel also increases, resulting in a rise in turbine productivity. Since the gas turbine's output dominates other productions in the system, the net electric power produced also increases. However, the exergy efficiency, defined as the ratio between the produced power and the exergy of input fuel, remains constant. An increase in the inlet fuel leads to a rise in the turbine outlet temperature, indicating that more thermal energy comes out from the GT, resulting in more heat received by heat exchangers. Ultimately, this leads to more release heat from the SRC and ORC cycles, resulting in a rise in the cooling load produced in the ARC and LNG, as depicted in Fig. 5(a). The hydrogen production rate is associated with the net power generation since a constant fraction of the generated electricity is sent into the electrolyzer. As a result, the capacity of produced hydrogen increases by increasing the inlet air, as shown in Fig. 5(a). The normalized CO_2 emission is expressed as the ratio of the amount of discharged CO_2 to the amount of provided useful energy unit. Since both of them increase when the air and inlet fuel increase, this ratio remains constant. The total cost rate is related to the inlet fuel, resulting in a rise, while the LCOE and LCOH decrease by increasing the inlet air/fuel because the hydrogen and electricity cost rates are higher than their production rates. The diagrams of economic and environmental functions, such as LCOE, LCOH, total cost rate, and NE of CO_2, are presented in Fig. 5(b). In summary, the air mass flow rate plays a crucial role in determining the system's main outputs, and its relationship with the inlet fuel affects the turbine productivity, net electric power produced, exergy efficiency, cooling load, hydrogen production rate, normalized CO_2 emission, total cost rate, LCOE, and LCOH. The optimization of the air mass flow rate is essential in achieving an efficient and cost-effective system while minimizing its environmental impact.

The compressor pressure ratio of the gas turbine cycle is a critical factor in determining the performance and efficiency of the gas turbine. An enhancement in this parameter can lead to an improvement in the net electric power produced by the gas turbine, as well as its exergetic performance. This is because the input exergy remains constant while the output power increases, resulting in a more efficient conversion of energy. Furthermore, an increase in the pressure ratio can also lead to an increase in hydrogen production. This is because the amount of net electric power generated by the gas turbine strongly influences the capacity of output hydrogen. However, this increase in net power production can lead to a decrease in the cooling load produced in the ARC and LNG, as the amount of heat received by heat exchangers decreases. Fig. 6(a) contains diagrams related to energy analysis that provide a visual representation of the relationship between pressure ratio, net power, hydrogen production, total cooling load, and exergy efficiency. These diagrams can help engineers and researchers better understand the performance and efficiency of gas turbines at varying pressure ratios. It's important to note that enhancing the pressure ratio increases the total cost rate. This is because the price of the gas turbine package increases with higher pressure ratios. As a result, the levelized cost of electricity (LCOE) and the levelized cost of hydrogen (LCOH) may be mitigated due to these increased costs, despite the higher amounts of electricity and hydrogen produced. On the positive side, an increase in the pressure ratio doesn't necessarily mean an increase in CO_2 emissions. In fact, the amount of CO_2 emission remains constant while the provided energy increases, which means the normalized emission of CO_2 declines as well (as seen in Fig. 6(b)).

Fig. 7 represents the relationship between the effectiveness of

Table 10
Examining the findings of both the current investigation and other comparable studies pertaining to ORC and GT subsystems.

ORC	Parameter	Present study	Yari (Yari, 2010)	Error (%)
	Power (kJ/kg)	50.6	50.38	0.43
	η_{ex} (%)	49.76	49.06	1.41
Gas turbine cycle	Parameter	Present study	Moghimi et al (Chitgar and Moghimi, 2020).	Error (%)
	Power (MW)	37.92	37.25	1.77
	η_{ex} (%)	33.12	32	3.5

Table 11
Comparing the results of the present study and results reported by Mosaffa et al. (2017).

Parameter	Present study	Mosaffa et al (Mehrpooya et al., 2021).	Difference Ratio (%)
$W_{net}(MW)$	12.487	12.628	1.12
$\dot{Q}_G(MW)$	37.36	37.68	0.85
Exergetic efficiency (%)	37.4	37.5933.51	0.51
Energetic efficiency (%)	33.35	33.5137.59	0.48

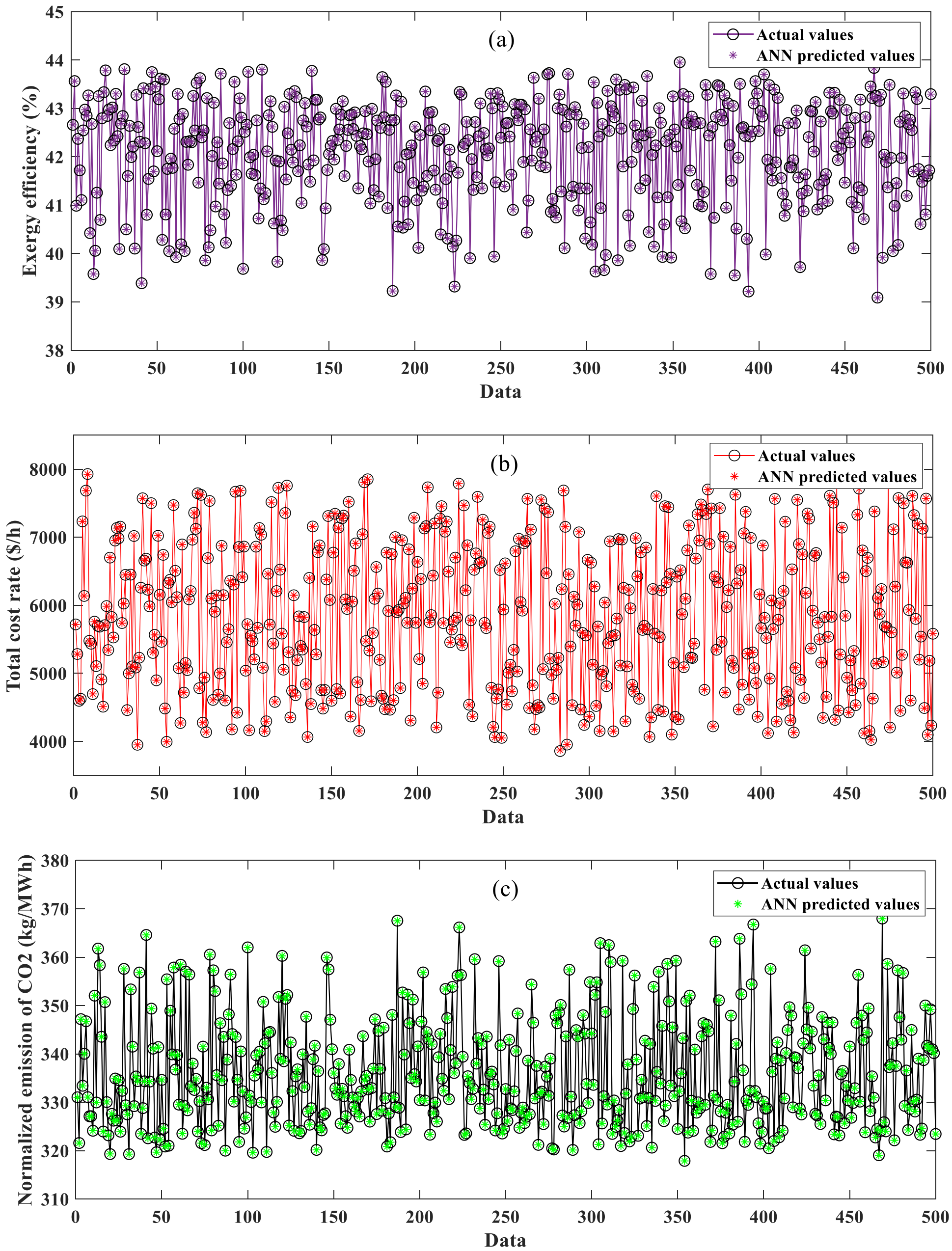

Fig. 4. Regressions for exergy efficiency (a), total cost rate (b), and normalized emission of CO_2 (c).

evaporator1 and the performance of a configured system. The effectiveness of evaporator1 refers to its ability to efficiently transfer heat from exhausted gases. When the effectiveness of evaporator1 improves, it means that more heat is extracted from the exhausted gases. This increased heat is then received by the steam Rankine cycle (SRC) and the absorption refrigeration cycle (ARC), resulting in an increase in the cooling load produced in the ARC. However, there are trade-offs associated with this improvement. As the temperature of the turbine outlet gas increases due to the higher heat transfer, less power can be generated in the gas turbine (GT). Additionally, less energy is received by the two organic Rankine cycles (ORCs), leading to reduced power generation in those subsystems as well. Consequently, the net power and exergy efficiency of the overall system decrease when the effectiveness of evaporator1 is increased. Since the production of hydrogen in the proton exchange membrane electrolyzer (PEME) is directly related to the net power production, an improvement in evaporator1 effectiveness results in a lower hydrogen production rate (as shown in Fig. 7(a)). The decrease in power production also affects the cost of components such as turbines or compressors, which decreases due to the reduced demand. Therefore, the total cost of the system declines. However, the levelized cost of electricity (LCOE) and the levelized cost of hydrogen (LCOH) increase because less electricity and hydrogen are being produced. Furthermore, the normalized emission of CO_2 rises because, with a constant emission level, the available energy for power generation decreases (as shown in Fig. 7(b)). In summary, improving the effectiveness of evaporator1 in the configured system has a complex impact on various factors such as cooling load, power generation, hydrogen production, cost, and CO_2 emissions.

The inlet pressure of the SRC plays a crucial role in determining the net power generation, exergy efficiency, and hydrogen production of the overall system. While the inlet pressure does not directly impact the gas turbine (GT), it does affect the SRC and ARC. An increase in the inlet pressure of the SRC results in an increase in net power generation, as shown in Fig. 8(a). This is because the power generated in the SRC

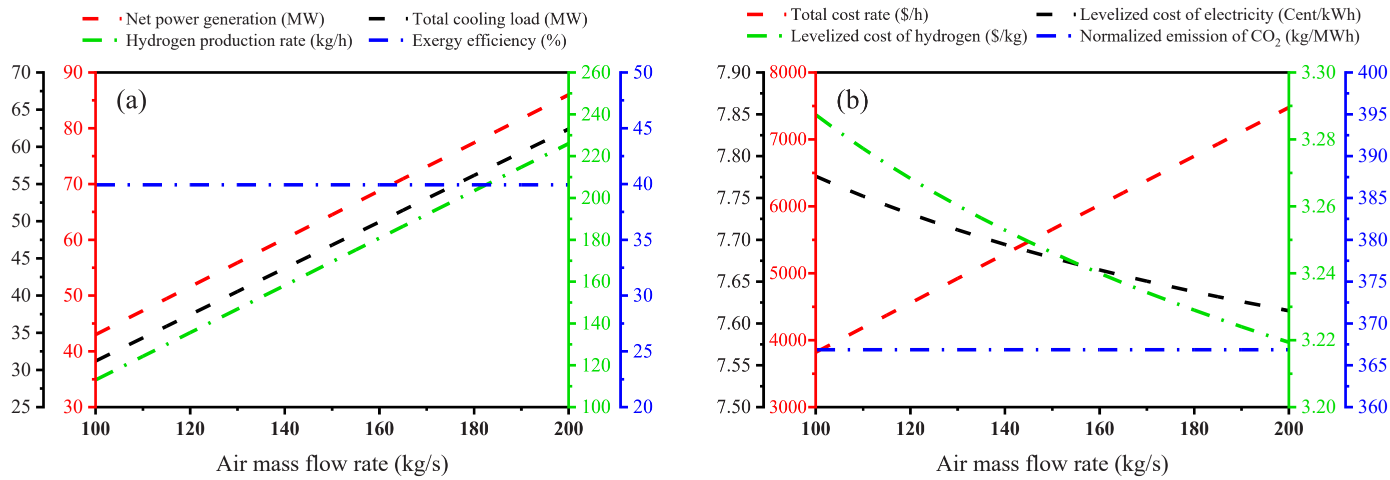

Fig. 5. The effect of mass flow rate of inlet air in the GT on the model's outputs.

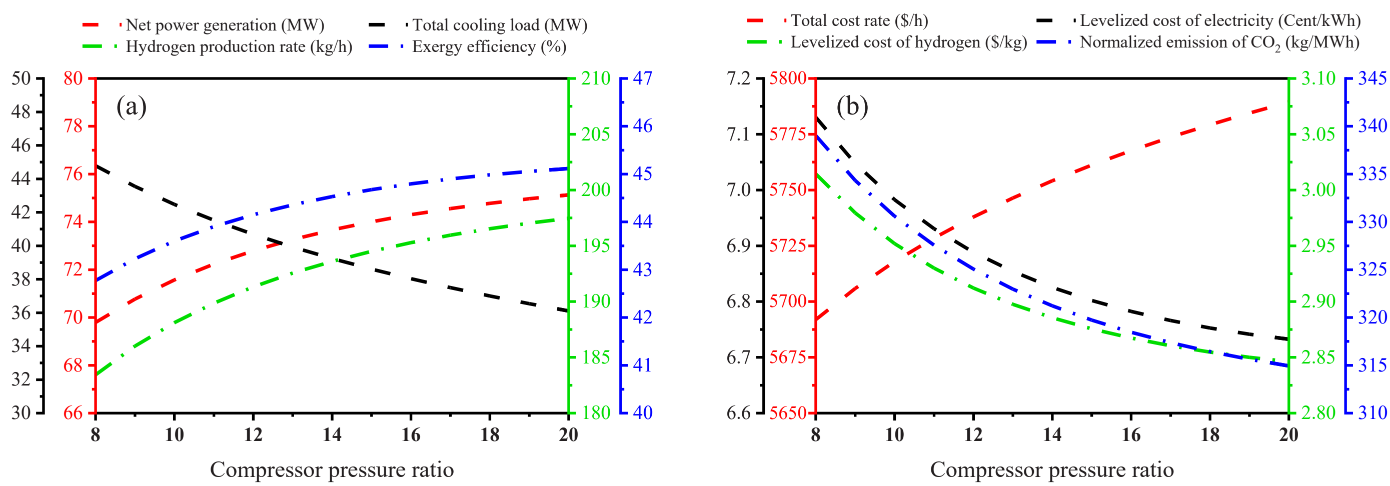

Fig. 6. The impact of compressor's pressure ratio on the model's main outputs.

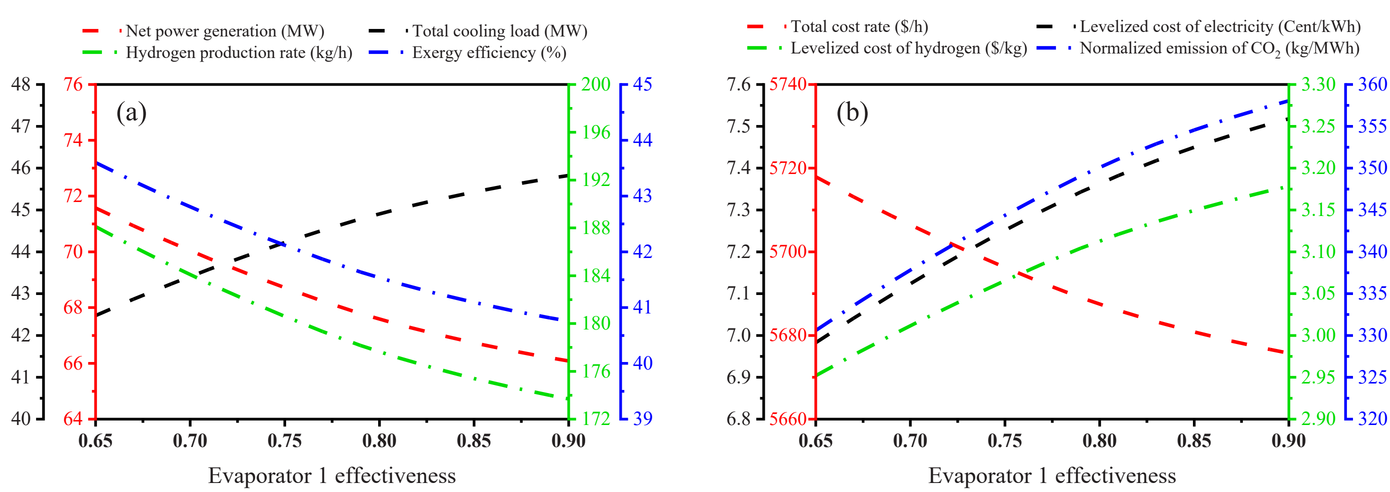

Fig. 7. The impact of evaporator 1 effectiveness on the system's main outputs.

turbine is enhanced when the inlet pressure increases while the outlet pressure remains constant. The increase in net output electricity also leads to an improvement in exergy efficiency. Furthermore, the hydrogen production rate follows the net power generation rate, meaning that an increase in inlet pressure leads to an increase in hydrogen production. However, the optimum pressure range for maximum net power generation, exergy efficiency, and hydrogen production appears to be between 3 and 4 MPa, as depicted in the

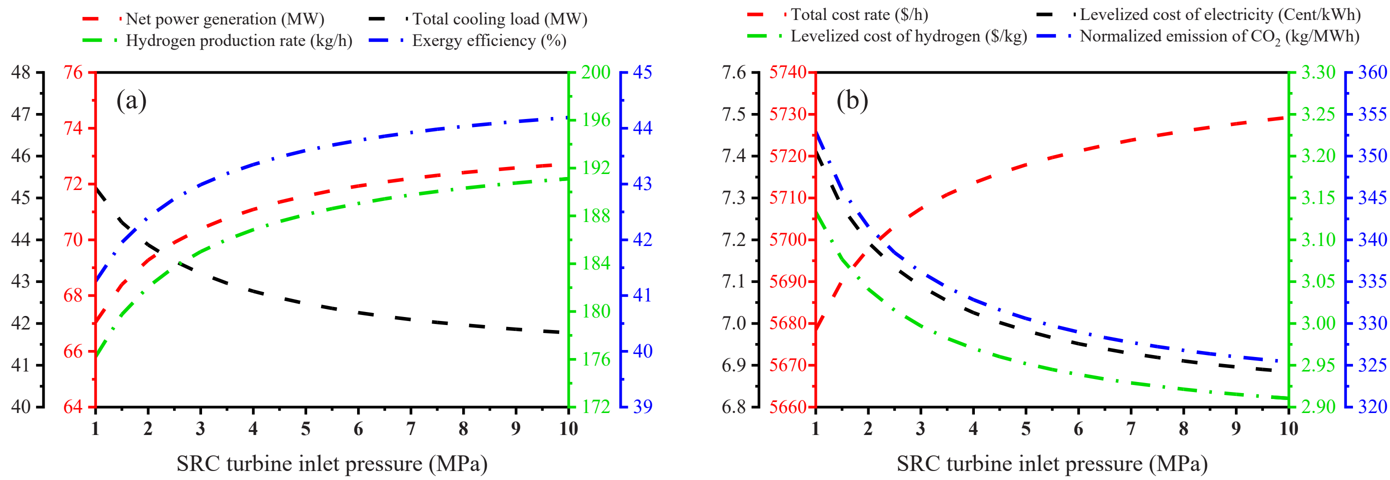

Fig. 8. Inlet pressure of SRC turbine variation and its impact on the system performance.

corresponding diagrams. Interestingly, increasing the inlet pressure also results in a decrease in the total cooling load. This is because the energy balance in evaporator1 leads to a lower water mass flow rate in the SRC, which results in less heat received by the ARC and a decrease in the cooling load produced. While increasing the net power leads to a higher total cost rate due to the increased price of the SRC turbine, the hydrogen production rate and electricity generation both increase. However, the amount of produced hydrogen or electricity is less than the cost of production. As a result, the levelized cost of electricity (LCOE) and the levelized cost of hydrogen (LCOH) decrease with an improvement in the inlet pressure. Simultaneously, normalized CO_2 emissions decline because the amount of CO_2 emitted remains constant while the amount of useful energy increases, as depicted in Fig. 8(b). Overall, the inlet pressure of the SRC plays a critical role in determining the performance and efficiency of the overall system. The optimum pressure range must be carefully balanced with the cost of production to achieve maximum efficiency and profitability.

Fig. 9 presents the results of the impact of the LNG turbine's inlet pressure on the model's key outputs. An increase in the LNG turbine's inlet pressure leads to an increase in net power production, resulting in an improvement in the generated electricity in the LNG turbine. Furthermore, this increase leads to a subsequent increase in the total exergetic efficiency and output hydrogen, as previously discussed. It is important to note that a portion of the cooling load comes from the LNG cooling unit, resulting in a growth in the total cooling production capacity due to the rising released cooling load in the LNG with higher pressure, as shown in Fig. 9(a). As the power generated by the LNG turbine increases, the price of electricity may become more expensive, resulting in a rise in the total cost rate. However, despite the increase in cost, the LCOE and LCOH decrease because the amount of produced hydrogen and electricity increases less than the rising production costs. Additionally, due to an increase in the amount of available energy relative to a constant emission rate of CO_2, the normalized CO_2 emission decreases. The impacts of varying the LNG turbine's inlet pressure on normalized CO_2 emissions, LCOH, LCOE, and total cost rate are demonstrated in Fig. 9(b). In conclusion, an increase in the LNG turbine's inlet pressure results in a rise in output electricity and efficiency at the expense of higher costs. However, this increase has a positive impact on CO_2 emissions due to the decrease in normalized CO_2 emission. Therefore, the optimization of the LNG turbine's inlet pressure is critical in achieving an efficient and environmentally friendly system.

5.3. The results of base system

This section of the report outlines the outcomes attained from the proposed model for the base design conditions, with a focus on the proposed system's 4E analysis. The input data considered for analyzing this scheme are presented in Table 12. Furthermore, Table 13 displays the thermodynamic conditions at various points throughout the cycle. According to the simulated model, the net output power of the proposed scheme is found to be 78.76 MW, as depicted in Table 14. According to the simulated model, the net output power of the proposed scheme is

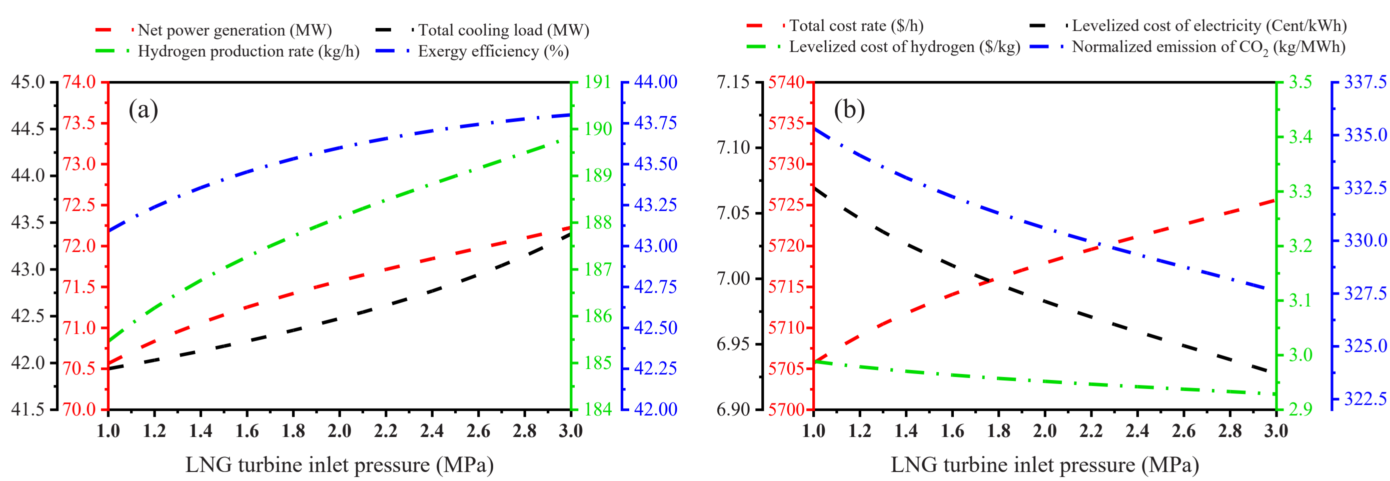

Fig. 9. The impact of LNG turbine inlet pressure on system performance.

Table 12
Input parameters of the proposed system.

Input data	Value
The reference pressure (MPa)	0.101
The reference temperature (K)	298.15
Compressor inlet pressure (MPa)	0.101
Compressor inlet temperature (K)	298.15
Gas turbine inlet temperature (K)	1473
Pressure ratio of compressor	10
Isentropic efficiency of air compressors (%)	85
Isentropic efficiency of gas turbine (%)	90
Inlet pressure of RC turbine (MPa)	5
Steam condensation pressure (MPa)	0.101
Efficiency of solution pump (%)	85
Effectiveness of solution HX (%)	85
Evaporator temperature (K)	278
Isentropic efficiency RC turbine and pump (%)	85
ORC1 turbine inlet pressure (MPa)	2.503
ORC1 turbine outlet pressure (MPa)	0.537
ORC2 turbine inlet pressure (MPa)	3
ORC2 turbine outlet pressure (MPa)	0.552
Isentropic efficiency of pumps and turbines of ORC units (%)	85
Inlet pressure of LNG turbine (MPa)	2
Natural gas network pressure (MPa)	0.3
Isentropic efficiency of turbine and pump (%)	85
P_{O_2} (kPa)	101.3
P_{H_2} (kPa)	101.3
T_{PEM} (K)	353
$E_{act,a}$ (kJ/mol)	76
$E_{act,c}$ (kJ/mol)	18
λ_a	14
λ_c	10
L (μm)	50
$J_a^{ref}(A/m^2)$	2×10^5
$J_c^{ref}(A/m^2)$	4.6×10^3

respectively.

Table 13
Thermodynamic state at different locations of the system.

State	Fluid	P (kPa)	T (K)	h (kJ/kg)	s (kJ/kg.K)
1	Air	101.32	298.15	298.37	6.859
2	Air	812.26	458.46	460.20	6.695
3	Flue gas	812.26	1530.1	1673.4	7.989
4	Flue gas	104	1017.6	1066.6	8.144
5	Flue gas	104	500	503.33	7.376
6	Flue gas	102	323	323.54	6.938
8	Water	101.32	373.12	419.06	1.307
9	Water	2941.9	373.50	422.76	1309
10	Water	2941.9	505.92	1199.9	3.024
11	Water	101.32	373.12	1087.9	3.099
12	R-134a	537.5	291.14	224.65	1.086
13	R-134a	2503	292.25	226.42	1.087
14	R-134a	2503	490	603.62	2.110
15	R-134a	537.5	436.59	554.31	2.123
16	Ethane	552	223.16	-571.27	-2.923
17	Ethane	3000	223.37	-569.06	-2.936
18	Ethane	3000	416.58	240.09	-0.331
19	Ethane	552	333.91	56.35	-0.281
21	LNG	101	111.74	-13.4	0.02
22	LNG	6500	114.4	4.7	0.05
23	LNG	6500	213.15	498.2	2.91
24	LNG	6500	283.15	774.6	4.10
25	LNG	3000	236.33	704.1	4.15
26	LNG	3000	236.33	704.1	4.15
28	Water	101.32	353	334.43	1.074
29	Oxygen	101.32	353	-	-
30	Hydrogen	101.32	353	4720.6	55.805

found to be 78.76 MW, as depicted in Table 14. This power output is composed of contributions from several sources, including 55.84 MW from gas turbines, 11.39 MW from SRCs, 7.48 MW from ORCs, and 4.05 MW from LNG units. The proposed system not only generates power but also allocates a portion of that power to an electrolysis unit, which produces hydrogen. In the specified conditions, the production capacity of hydrogen equals 185.15 kg/h. Based on Eqs. (13) and (14), the levelized cost of electricity (LCOE) and levelized cost of hydrogen (LCOH) are calculated to be 7.09 cents/kWh and 2.99 $/kg, respectively. From an environmental perspective, the system's normalized CO2 emission is estimated to be 335.89 kg/MWh. The cooling load production, which is the sum of the cooling yielded by ARC and LNG cooling loads, is estimated to be 38.65 MW. This cooling is utilized for local cooling purposes. Finally, the report provides additional information on the exergetic efficiency and total cost rate of the scheme, which are obtained to be 39.03% and 5715.3 $/h,

Table 14
Results of the base cycle.

Parameter	value
Gas turbine output power	55.84 MW
SRC output power	11.39 MW
ORCs output power	7.48 MW
LNG turbine output power	4.05 MW
Cooling load	38.65 MW
LCOE	7.09 Cent/kWh
LCOH	2.99 $/kg
Normalized emission of CO_2	335.89 kg/MWh
Exergy efficiency	39.03%
Total rate of cost	5715.3 $/h
Capacity of produced hydrogen	185.15 kg/h

5.4. Results of optimization

In the optimization of energy systems, the Pareto frontier represents the set of optimal solutions that balance multiple objectives, such as cost, efficiency, and environmental impact. The concept is useful in energy system design and planning, where multiple conflicting objectives must be considered. The Pareto frontier allows designers to identify trade-offs between different objectives and select the most appropriate solution for their specific needs. The Pareto frontier has been applied to optimize energy systems in various applications, including renewable energy systems, power generation, and industrial processes. The outcomes of the present study specify that the output parameters of certain schemes are influenced by their design parameters. Additionally, it was observed that some design parameters have a stronger effect on the system's performance compared to others, which is referred to as sensitivity of the main outputs of the system on design parameters. To achieve optimal system performance, an optimization method must be employed. In this particular study, a GA optimization technique was utilized and the results are presented in Fig. 10. This figure displays the outcome of the optimization process, which helped identify the best possible performance for the system being studied.

In the GA optimization process, the last generation of each GA optimization comprises a population for each decision variable. These populations represent the distribution of genes for each decision variable, with each population indicating a certain value that can be considered as optimal value for that particular variable. The distribution of these populations has been illustrated through Fig. 11, which displays the optimum values for each variable. Essentially, Fig. 11 presents the population distribution for each decision variable and highlights the optimal value for each one. By identifying the optimum value for each decision variable, the GA optimization technique allows for the determination of the best possible combination of values for all variables, resulting in optimal system performance. Overall, the presentation of this data through Fig. 11 provides valuable insights into the GA optimization process and emphasizes the importance of determining the optimal values for each decision variable to accomplish optimum system performance.

Table 15 provides a comprehensive list of the optimal values of each decision variable and the primary outputs generated by the model. The

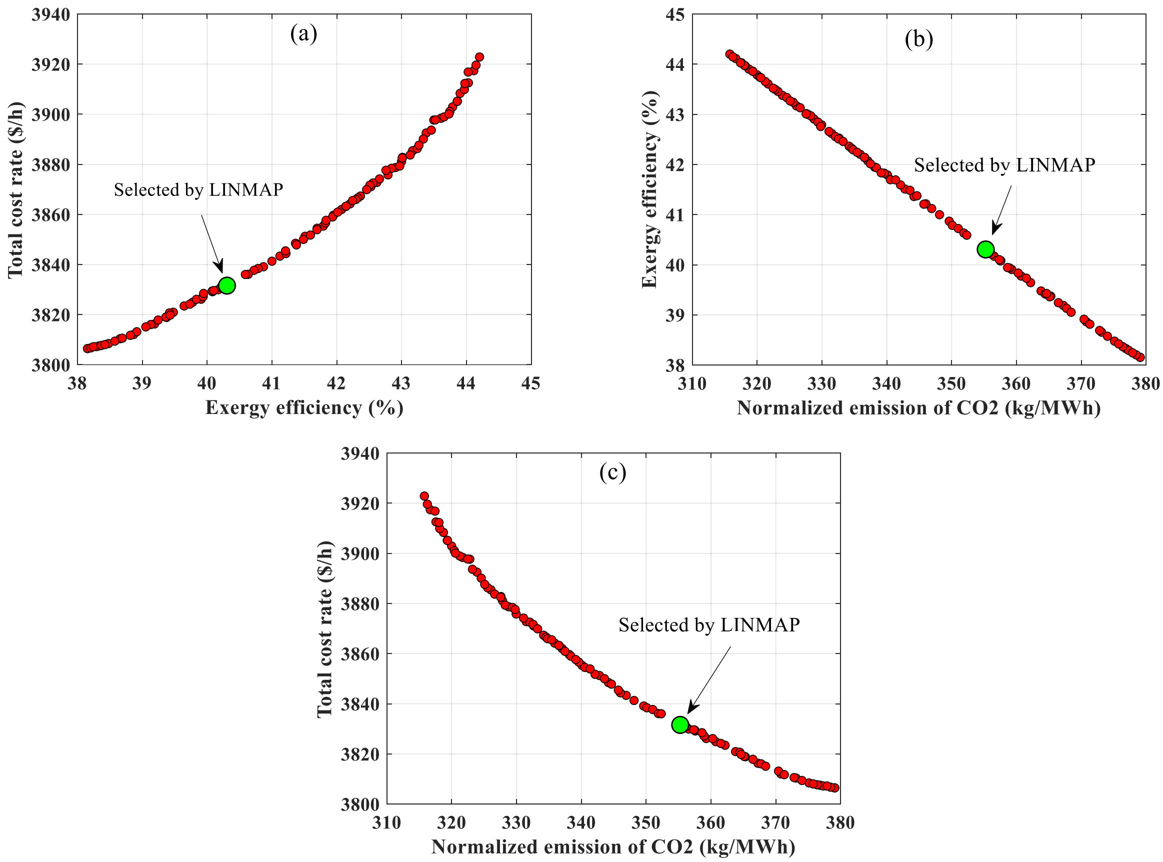

Fig. 10. Pareto front of three objective functions, total cost rate versus exergy efficiency (a), exergy efficiency versus normalized CO_2 emission (b), and total cost rate versus normalized CO_2 emission (c).

optimization process resulted in the attainment of optimum design parameters for five decision variables, which are presented in the output table. Following this, the optimized scenario was recalculated using the model, with the resultant values for system main outputs and objective functions recorded. This process allowed for an evaluation of the effectiveness of the optimization process and provided insights into the system performance under the optimal situation.

To find more about the result and the influence of parameters on the system's main criteria, a sensitivity analysis has also been conducted as it is presented in Fig. 12. The figure shows that air inlet mass flow rate has the most impact on the cost because of the cost of the fuel which dominates other costs. However, other parameters have more impact on the exergy efficiency and normalized emission of CO_2 other than total cost rate.

6. Conclusion

The intended goal of this proposed system is to create power, produce cooling load, and generate hydrogen by utilizing various subsystems such as a gas turbine, an SRC, two ORCs, an LNG, an ARC, and a PEM electrolyzer to enable hydrogen generation and storage. The proposed system takes advantage of the expandability of LNG for extra power generation and its cooling load. Coupling the LNG regasification process with a multigeneration gas turbine power plant can offer several benefits, including increased energy efficiency, lower costs, and reduced environmental impact. The gas turbine's waste heat can be recovered and used for various applications like cooling and electricity generation, resulting in higher overall efficiency of the plant. This integrated approach also enhances the flexibility and reliability of the plant, allowing it to meet varying demand requirements efficiently. Additionally, it helps reduce greenhouse gas emissions, making it an environmentally sustainable solution for meeting energy needs. In order to conduct calculations for a base case scenario, a MATLAB function was employed. Subsequently, to make the system more viable for implementation and determine its feasibility, a GA optimization technique was utilized with the aid of a machine learning model to minimize runtime.

The current study has accomplished significant achievements that have been methodically classified into the following categories:

- Co-utilization of the LNG regasification process with multigeneration gas turbine power plants offered a sustainable solution to meeting energy needs by minimizing greenhouse gas emissions and supporting sustainable development.
- Changing the flow rate of the inlet air between 100 and 200 kg/s has resulted in varying the hydrogen capacity and net power production between 112 and 225 kg/h and 44–85 MW, respectively. This variation caused a decrease in LCOE by 0.15 Cent/kWh and LCOH by 0.07 $/kg.
- The pressure ratio of compressor adjustments from 6 to 18 resulted in a change in cooling load from 45 to 36 MW. However, the variations in pressure ratio led to a decrease in LCOE by 0.4 Cent/kWh and LCOH by 0.15 $/kg.
- By changing the turbine inlet pressure of the SRC system from 1 to 10 MPa, the net power varied from 67 to 72 MW, exergy efficiency ranged from 41% to 44%, total cost rate altered from 5680 to 5725 $/h, and Normalized CO_2 emission changed from 350 to 325 kg/GJ.
- An increase in the LNG turbine's inlet pressure led to increasing the net output electricity, exergy efficiency and hydrogen production rate. However, it increased the total cooling load and cost rate, while decreasing LCOE and LCOH. The normalized CO_2 emission decreased

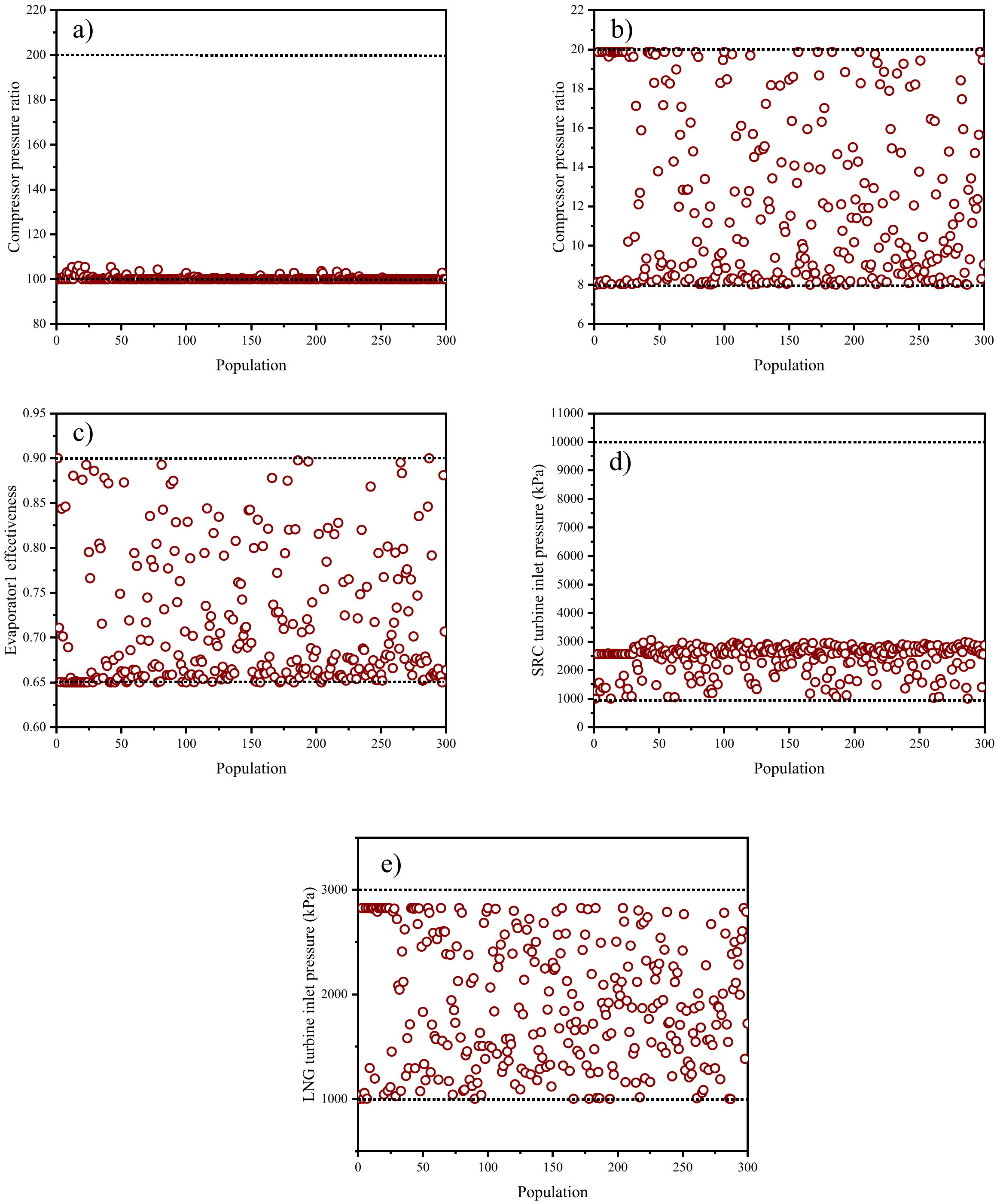

Fig. 11. Distribution of genes for each decision variable.

Table 15
The optimal value of system input and output parameters.

Parameter	Value
Optimum Design parameters	
Pressure ratio of compressor	8.18
Air flow rate (kg/s)	100
Evaporator1 effectiveness	0.69
Inlet pressure of SRC turbine (MPa)	2.94
Inlet pressure of LNG turbine (MPa)	1.35
Objective functions	
Exergetic efficiency (%)	40.32
Total rate of cost ($/h)	3830.8
Normalized emission of CO_2 (kg/MWh)	355

owing to an increase in available energy, indicating a positive impact on CO_2 emissions.

- Post optimization of the system performance, the achieved results for exergy efficiency, total cost rate, and normalized CO_2 emission were 40.32%, 3830.8 $/h, and 355 kg/GJ, respectively.
- Finally, the use of ANN has reduced the optimization run-time from 47 h to 16 min.

6.1. Recommendations

Storing and transporting hydrogen in its gaseous state face several limitations. Hydrogen gas has low energy density and takes up a large

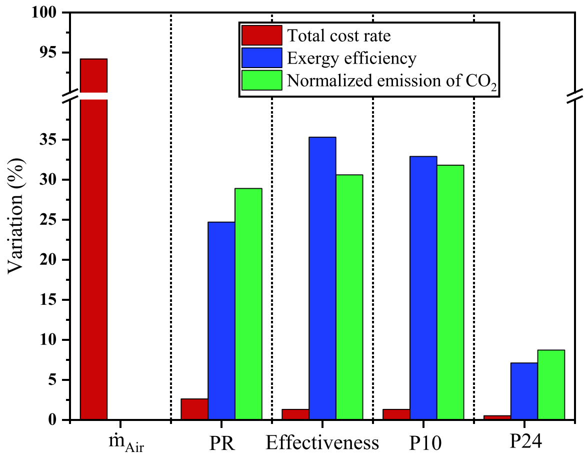

Fig. 12. Sensitivity analysis.

volume, making it impractical for certain applications. Also, high-pressure storage requirements pose safety concerns and require specialized infrastructure. It should be noted that hydrogen gas is highly flammable and prone to leakage, increasing the risk of accidents. Moreover, long-distance transportation of hydrogen gas can be inefficient and expensive due to the need for dedicated pipelines or high-pressure tanks. The limitations highlight the importance of exploring alternative methods such as liquid or solid-state hydrogen carriers for more practical storage and transportation solutions. In this regard, It is recommended that forthcoming research endeavors explore the viability of storing hydrogen in a liquid state, and thoroughly investigate various liquefaction techniques within the proposed framework.

Declaration of Competing Interest

The authors declare that they have no known competing financial interests or personal relationships that could have appeared to influence the work reported in this paper.

Acknowledgements

Authors acknowledge financial support from Abu Dhabi University's Office of Research and Sponsored Programs. Grant number: 19300767. This study is supported via funding from Prince Sattam bin Abdulaziz University project number (PSAU/2023/R/1444).

References

Abbasi, H.R., Pourrahmani, H., 2020. Multi-criteria optimization of a renewable hydrogen and freshwater production system using HDH desalination unit and thermoelectric generator. Energy Convers. Manag 214, 112903.

Abbasi, M., Chahartaghi, M., Hashemian, S.M., 2018. Energy, exergy, and economic evaluations of a CCHP system by using the internal combustion engines and gas turbine as prime movers. Energy Convers. Manag 173, 359–374. https://doi.org/10.1016/j.enconman.2018.07.095.

Ahmadi, P., Dincer, I., Rosen, M.A., 2013. Energy and exergy analyses of hydrogen production via solar-boosted ocean thermal energy conversion and PEM electrolysis. Int J. Hydrog. Energy 38, 1795–1805. https://doi.org/10.1016/J.IJHYDENE.2012.11.025.

Alali, A.E., Al, Khasawneh, Tubeshat A., Al, K., 2022. Performance analysis of stirling engine double-effect absorption chiller hybrid system for waste heat utilization from gas turbine modular helium reactor. Energy Convers. Manag 251, 114976. https://doi.org/10.1016/J.ENCONMAN.2021.114976.

Alirahmi, S.M., Bashiri Mousavi, S., Razmi, A.R., Ahmadi, P., 2021. A comprehensive techno-economic analysis and multi-criteria optimization of a compressed air energy storage (CAES) hybridized with solar and desalination units. Energy Convers. Manag 236, 114053. https://doi.org/10.1016/j.enconman.2021.114053.

Ates, F., Ozcan, H., 2022. Turkey's industrial waste heat recovery potential with power and hydrogen conversion technologies: A techno-economic analysis. Int J. Hydrog. Energy 47, 3224–3236. https://doi.org/10.1016/J.IJHYDENE.2020.11.059.

Bamisile, O., Cai, D., Adedeji, M., Dagbasi, M., Li, J., Hu, Y., et al., 2023. Thermo-enviro-exergoeconomic analysis and multi-objective optimization of a novel geothermal-solar-wind micro-multi-energy system for cleaner energy production. Process Saf. Environ. Prot. 170, 157–175. https://doi.org/10.1016/J.PSEP.2022.11.068.

Behnam, P., Arefi, A., Shafii, M.B., 2018. Exergetic and thermoeconomic analysis of a trigeneration system producing electricity, hot water, and fresh water driven by low-temperature geothermal sources. Energy Convers. Manag 157, 266–76.

Bejan, A., Tsatsaronis, G., Moran, M.J., 1995. Thermal Design and Optimization. John Wiley & Sons,.

Cao, Y., Dhahad, H.A., Togun, H., Hussen, H.M., Anqi, A.E., Farouk, N., et al., 2021. Effect of working fluids in a novel geothermal-based integration of organic-flash and power/cooling generation cycles with hydrogen and freshwater production units. Int J. Hydrog. Energy 46, 28370–28386. https://doi.org/10.1016/J.IJHYDENE.2021.06.129.

Chitgar, N., Moghimi, M., 2020. Design and evaluation of a novel multi-generation system based on SOFC-GT for electricity, fresh water and hydrogen production. Energy 197, 117162. https://doi.org/10.1016/j.energy.2020.117162.

Delpisheh, M., Haghghi, M.A., Athari, H., Mehrpooya, M., 2021. Desalinated water and hydrogen generation from seawater via a desalination unit and a low temperature electrolysis using a novel solar-based setup. Int J. Hydrog. Energy 46, 7211–7229. https://doi.org/10.1016/j.ijhydene.2020.11.215.

Emadi, M.A., Mahmoudimehr, J., 2019. Modeling and thermo-economic optimization of a new multi-generation system with geothermal heat source and LNG heat sink. Energy Convers. Manag 189, 153–66.

Haghghi, M.A., Hasanzadeh, A., Nadimi, E., Rosato, A., Athari, H., 2023a. An Intelligent Thermodynamic/Economic Approach Based on Artificial Neural Network Combined with MOGWO Algorithm to Study a Novel Polygeneration Scheme Using a Modified Dual-Flash Geothermal Cycle. Process Saf. Environ. Prot.

Haghghi, M.A., Mohammadi, Z., Delpisheh, M., Nadimi, E., Athari, H., 2023b. Multi-variable study/optimization of a novel geothermal-driven poly-generation system: Application of a soft-computing intelligent procedure and MOGWO. Process Saf. Environ. Prot. 171, 507–531. https://doi.org/10.1016/j.psep.2023.01.041.

Khanmohammadi, S., Atashkari, K., Kouhikamali, R., 2015. Exergoeconomic multi-objective optimization of an externally fired gas turbine integrated with a biomass gasifier. Appl. Therm. Eng. 91, 848–59.

Khanmohammadi, S., Heidarnejad, P., Javani, N., Ganjehsarabi, H., 2017. Exergoeconomic analysis and multi objective optimization of a solar based integrated energy system for hydrogen production. Int J. Hydrog. Energy 42, 21443–21453. https://doi.org/10.1016/j.ijhydene.2017.02.105.

Li, H.M., Li, G.X., Li, L., 2023. Comparative investigation on combustion characteristics of ADN-based liquid propellants in inert gas and oxidizing gas atmospheres with resistive ignition method. Fuel 334, 126742. https://doi.org/10.1016/J.FUEL.2022.126742.

Liu, F., Sun, Z., Bian, H., Ding, M., Meng, X., 2023. Identification and classification of the flow pattern of hydrogen-air-steam mixture gas under steam condensation. Int J. Therm. Sci. 183, 107854 https://doi.org/10.1016/J.IJTHERMALSCI.2022.107854.

Liu, L., Tang, Y., Liu, D., 2022a. Investigation of future low-carbon and zero-carbon fuels for marine engines from the view of thermal efficiency. Energy Rep. 8, 6150–6160. https://doi.org/10.1016/J.EGYR.2022.04.058.

Liu, L., Wu, Y., Wang, Y., Wu, J., Fu, S., 2022b. Exploration of environmentally friendly marine power technology -ammonia/diesel stratified injection. J. Clean. Prod. 380, 135014 https://doi.org/10.1016/J.JCLEPRO.2022.135014.

Lu, N., Pan, L., Liu, Z., Lee, K.Y., Song, Y., Si, P., 2020. Dynamic modeling of thermal-supply system for two-by-one combined-cycle gas and steam turbine unit. Fuel Process Technol. 209, 106549 https://doi.org/10.1016/j.fuproc.2020.106549.

Maheshwari, M., Singh, O., 2019. Comparative evaluation of different combined cycle configurations having simple gas turbine, steam turbine and ammonia water turbine. Energy 168, 1217–1236. https://doi.org/10.1016/j.energy.2018.12.008.

Mehdikhani, V., Mirzaee, I., Khalilian, M., Abdolalipouradl, M., 2022. Thermodynamic and exergoeconomic assessment of a new combined power, natural gas, and hydrogen system based on two geothermal wells. Appl. Therm. Eng. 206, 118116 https://doi.org/10.1016/j.applthermaleng.2022.118116.

Mehrenjani, J.R., Gharehghani, A., Nasrabadi, A.M., Moghimi, M., 2022a. Design, modeling and optimization of a renewable-based system for power generation and hydrogen production. Int J. Hydrog. Energy 47, 14225–14242. https://doi.org/10.1016/j.ijhydene.2022.02.148.

Mehrenjani, J.R., Gharehghani, A., Sangesaraki, A.G., 2022b. Machine learning optimization of a novel geothermal driven system with LNG heat sink for hydrogen production and liquefaction. Energy Convers. Manag 254, 115266. https://doi.org/10.1016/j.enconman.2022.115266.

Mehrpooya, M., Ansarinasab, H., Mousavi, S.A., 2021. Life cycle assessment and exergoeconomic analysis of the multi-generation system based on fuel cell for methanol, power, and heat production. Renew. Energy 172, 1314–1332. https://doi.org/10.1016/j.renene.2021.03.111.

Miao, Z., Meng, X., Liu, L., 2021. Design a new thermoelectric module with high practicability based on experimental measurement. Energy Convers. Manag 241, 114320. https://doi.org/10.1016/J.ENCONMAN.2021.114320.

Moghimi, M., Emadi, M., Ahmadi, P., Moghadasi, H., 2018. 4E analysis and multi-objective optimization of a CCHP cycle based on gas turbine and ejector refrigeration. Appl. Therm. Eng. 141, 516–530. https://doi.org/10.1016/j.applthermaleng.2018.05.075.

Mosaffa, A.H., Mokarram, N.H., Farshi, L.G., 2017. Thermo-economic analysis of combined different ORCs geothermal power plants and LNG cold energy. Geothermics 65, 113–125. https://doi.org/10.1016/j.geothermics.2016.09.004.

Nasrabadi, A.M., Korpeh, M., 2023. Techno-economic analysis and optimization of a proposed solar-wind-driven multigeneration system; case study of Iran. Int J. Hydrog. Energy. https://doi.org/10.1016/j.ijhydene.2022.12.283.

Nasrabadi, A.M., Moghimi, M., 2022. Energy analysis and optimization of a biosensor-based microfluidic microbial fuel cell using both genetic algorithm and neural network PSO. Int J. Hydrog. Energy 47, 4854–4867. https://doi.org/10.1016/j.ijhydene.2021.11.125.

Nasrabadi, A.M., Malaei, O., Moghimi, M., Sadeghi, S., Hosseinalipour, S.M., 2022a. Deep learning optimization of a combined CCHP and greenhouse for CO_2 capturing; case study of Tehran. Energy Convers. Manag 267, 115946. https://doi.org/10.1016/j.enconman.2022.115946.

Nasrabadi, A.M., Malaei, O., Moghimi, M., Sadeghi, S., Hosseinalipour, S.M., 2022b. Deep learning optimization of a combined CCHP and greenhouse for CO_2 capturing; case study of Tehran. Energy Convers. Manag 267, 115946. https://doi.org/10.1016/j.enconman.2022.115946.

Olumayegun, O., Wang, M., Kelsall, G., 2016. Closed-cycle gas turbine for power generation: A state-of-the-art review. Fuel 180, 694–717. https://doi.org/10.1016/j.fuel.2016.04.074.

Pátek, J., Klomfar, J., 2006. A computationally effective formulation of the thermodynamic properties of LiBr–H2O solutions from 273 to 500 K over full composition range. Int J. Refrig 29, 566–578. https://doi.org/10.1016/J.IJREFRIG.2005.10.007.

Pourrahmani, H., Moghimi, M., 2019. Exergoeconomic analysis and multi-objective optimization of a novel continuous solar-driven hydrogen production system assisted by phase change material thermal storage system. Energy 189, 116170.

Razmi, A.R., Alirahmi, S.M., Nabat, M.H., Assareh, E., Shahbakhti, M., 2022. A green hydrogen energy storage concept based on parabolic trough collector and proton exchange membrane electrolyzer/fuel cell: Thermodynamic and exergoeconomic analyses with multi-objective optimization. Int J. Hydrog. Energy. https://doi.org/10.1016/J.IJHYDENE.2022.03.021.

Shakibi, H., Nedaei, N., Farajollahi, A.H., Chitsaz, A., 2023. Exergoeconomic appraisement, sensitivity analysis, and multi-objective optimization of a solar-driven generation plant for yielding electricity and cooling load. Process Saf. Environ. Prot. 170, 89–111. https://doi.org/10.1016/J.PSEP.2022.11.067.

Strušnik, D., Avsec, J., 2022. Exergoeconomic machine-learning method of integrating a thermochemical Cu–Cl cycle in a multigeneration combined cycle gas turbine for hydrogen production. Int J. Hydrog. Energy 47, 17121–17149. https://doi.org/10.1016/j.ijhydene.2022.03.230.

Sun, X., Chen, Z., Sun, Z., Wu, S., Guo, K., Dong, Z., et al., 2023b. High-Efficiency utilization of waste shield slurry: A geopolymeric Flocculation-Filtration-Solidification method. Constr. Build. Mater. 387, 131569 https://doi.org/10.1016/J.CONBUILDMAT.2023.131569.

Sun, Z., Wang, T., Zhang, R., Li, H., Wu, Y., Toan, S., et al., 2023a. Boosting hydrogen production via deoxygenation-sorption-enhanced biomass gasification. Bioresour. Technol. 382, 129197 https://doi.org/10.1016/J.BIORTECH.2023.129197.

Tahir, M.F., Haoyong, C., Guangze, H., 2021. A comprehensive review of 4E analysis of thermal power plants, intermittent renewable energy and integrated energy systems. Energy Rep. 7, 3517–3534. https://doi.org/10.1016/j.egyr.2021.06.006.

Wang, B., Gupta, R., Bei, L., Wan, Q., Sun, L., 2023. A review on gasification of municipal solid waste (MSW): Syngas production, tar formation, mineral transformation and industrial challenges. Int J. Hydrog. Energy. https://doi.org/10.1016/J.IJHYDENE.2023.03.086.

Wang, Y., Cao, Q., Liu, L., Wu, Y., Liu, H., Gu, Z., et al., 2022. A review of low and zero carbon fuel technologies: Achieving ship carbon reduction targets. Sustain Energy Technol. Assess. 54, 102762 https://doi.org/10.1016/J.SETA.2022.102762.

Xia C., Zhu Y., Zhou S., Peng H., Feng Y., Zhou W., et al. Simulation study on transient performance of a marine engine matched with high-pressure SCR system. Https://DoiOrg/101177/14680874221084052 2022;24:1327–45. https://doi.org/10.1177/14680874221084052.

Xiao, G., Chen, J., Ni, M., Cen, K., 2021. A solar micro gas turbine system combined with steam injection and ORC bottoming cycle. Energy Convers. Manag 243, 114032. https://doi.org/10.1016/j.enconman.2021.114032.

Yari, M., 2010. Exergetic analysis of various types of geothermal power plants. Renew. Energy 35, 112–121. https://doi.org/10.1016/j.renene.2009.07.023.

Yilmaz, F., Ozturk, M., 2022. Thermodynamic and economic investigation of an innovative multigeneration plant integrated with the solar collector and combustion chamber. Int J. Hydrog. Energy. https://doi.org/10.1016/J.IJHYDENE.2022.02.204.

Yilmaz, F., Ozturk, M., Selbas, R., 2020. Design and thermodynamic modeling of a renewable energy based plant for hydrogen production and compression. Int J. Hydrog. Energy 45, 26126–26137. https://doi.org/10.1016/j.ijhydene.2019.12.133.

You, H., Han, J., Liu, Y., Chen, C., Ge, Y., 2020a. 4E analysis and multi-objective optimization of a micro poly-generation system based on SOFC/MGT/MED and organic steam ejector refrigerator. Energy 206. https://doi.org/10.1016/j.energy.2020.118122.

You, H., Han, J., Liu, Y., 2020b. Conventional and advanced exergoeconomic assessments of a CCHP and MED system based on solid oxide fuel cell and micro gas turbine. Int J. Hydrog. Energy 45, 12143–12160. https://doi.org/10.1016/J.IJHYDENE.2020.02.138.

Zahedi, R., Ahmadi, A., Dashti, R., 2021. Energy, exergy, exergoeconomic and exergoenvironmental analysis and optimization of quadruple combined solar, biogas, SRC and ORC cycles with methane system. Renew. Sustain Energy Rev. 150, 111420 https://doi.org/10.1016/j.rser.2021.111420.

Zang, G., Jia, J., Tejasvi, S., Ratner, A., Silva Lora, E., 2018. Techno-economic comparative analysis of Biomass Integrated Gasification Combined Cycles with and without CO_2 capture. Int J. Greenh. Gas. Control 78, 73–84. https://doi.org/10.1016/j.ijggc.2018.07.023.

Zhao, Y., Liu, G., Li, L., Yang, Q., Tang, B., Liu, Y., 2019. Expansion devices for organic Rankine cycle (ORC) using in low temperature heat recovery: A review. Energy Convers. Manag 199, 111944. https://doi.org/10.1016/j.enconman.2019.111944.

Zuo, L., Yu, S., Zhang, R., Li, H., Wu, Y., Abiev, R., et al., 2023. Tunning Pd–Cu-based catalytic oxygen carrier for intensifying low-temperature methanol reforming. J. Clean. Prod. 410, 137212 https://doi.org/10.1016/J.JCLEPRO.2023.137212.